UNCLASSIFIED

AD NUMBER
ADB025447
LIMITATION CHANGES
TO: **Approved for public release; distribution is unlimited.**
FROM: **Distribution authorized to U.S. Gov't. agencies only; Test and Evaluation; 30 JAN 1978. Other requests shall be referred to Electronic Systems Devision, Attn: AFSC, Hanscom AFB, MS 01731.**
AUTHORITY
ESD ltr, 5 Jul 1978

THIS PAGE IS UNCLASSIFIED

2
B.S

Semiannual Technical Report 13

TECHNICAL SUPPORT FOR THE CONUS OTH-B EXPERIMENTAL RADAR SYSTEM

By: W. B. ZAVOLI T. W. WASHBURN P. C. EVANS C. A. COLE

Prepared for:

ELECTRONIC SYSTEMS DIVISION (AFSC)
USAF 414L SYSTEM PROGRAM OFFICE
HANSCOM AFB, MASSACHUSETTS 01731

CONTRACT N00014-75-C-0930
(NR 088-076)

Distribution limited to U.S. Government agencies only; Test and Evaluation, 30 January 1978. Other requests for this document must be referred to the USAF 414L System Program Office, Electronic Systems Division (AFSC), Hanscom AFB, Massachusetts 01731.

This research was sponsored by the Electronic Systems Division, Air Force Systems Command, and was monitored by the Office of Naval Research under Contract No. N00014-75-C-0930 (NR 088-076).

333 Ravenswood Avenue
Menlo Park, California 94025 U.S.A.
(415) 326-6200
Cable: STANRES, Menlo Park
TWX: 910-373-1246

SRI International

SRI International

Semiannual Technical Report 13
Covering the Period 1 January through 30 June 1977

December 1977

TECHNICAL SUPPORT FOR THE CONUS OTH-B EXPERIMENTAL RADAR SYSTEM

By: W. B. ZAVOLI T. W. WASHBURN P. C. EVANS C. A. COLE

Prepared for:

ELECTRONIC SYSTEMS DIVISION (AFSC)
USAF 414L SYSTEM PROGRAM OFFICE
HANSCOM AFB, MASSACHUSETTS 01731

CONTRACT N00014-75-C-0930
(NR 088-076)

SRI Project 4062

Distribution limited to U.S. Government agencies only; Test and Evaluation, 30 January 1978. Other requests for this document must be referred to the USAF 414L System Program Office, Electronic Systems Division (AFSC), Hanscom AFB, Massachusetts 01731.

This research was sponsored by the Electronic Systems Division, Air Force Systems Command, and was monitored by the Office of Naval Research under Contract No. N00014-75-C-0930 (NR 088-076).

Approved by:

L. E. SWEENEY, JR., *Director*
Remote Measurements Laboratory

RAY L. LEADABRAND, *Executive Director*
Electronics and Radio Sciences Division

Copy No. 14

SRI International
333 Ravenswood Avenue · Menlo Park, California 94025 · U.S.A.

UNCLASSIFIED

SECURITY CLASSIFICATION OF THIS PAGE (When Data Entered)

REPORT DOCUMENTATION PAGE

READ INSTRUCTIONS BEFORE COMPLETING FORM

1. REPORT NUMBER

2. GOVT ACCESSION NO.

3. RECIPIENT'S CATALOG NUMBER

no.

4. TITLE (and Subtitle)

6 TECHNICAL SUPPORT FOR THE CONUS OTH-B EXPERIMENTAL RADAR SYSTEM.

9

5. TYPE OF REPORT & PERIOD COVERED

Semiannual Technical Report 13,

~~Covering the period~~

1 Jan[redacted] 30 Jun[redacted]77,

6. ~~PERFORMING ORG. REPORT NUMBER~~

SRI Project 4062

7. AUTHOR(s)

10 Walter B./Zavoli, Taylor W./Washburn, Philip C./Evans, Charles A./Cole

8. CONTRACT OR GRANT NUMBER(s)

15 Contract N00014-75-C-0930, ARPA Order-1656

9. PERFORMING ORGANIZATION NAME AND ADDRESS

Stanford Research Institute
333 Ravenswood Avenue
Menlo Park, California 94025

10. PROGRAM ELEMENT, PROJECT, TASK AREA & WORK UNIT NUMBERS

ONR NR 088-076

11. CONTROLLING OFFICE NAME AND ADDRESS

Electronic Systems Division (AFSC)
USAF 414L System Program Office
Hanscom AFB, Massachusetts 01731

11

12. REPORT DATE

Dec[redacted]77

13. NO. OF PAGES

72

14. MONITORING AGENCY NAME & ADDRESS (if diff. from Controlling Office)

Office of Naval Research (Code 461(FP))
800 North Quincy Street
Arlington, Virginia 22217

15. SECURITY CLASS. (of this report)

UNCLASSIFIED 12 63P.

15a. DECLASSIFICATION/DOWNGRADING SCHEDULE

16. DISTRIBUTION STATEMENT (of this report)

Distribution limited to U.S. Government agencies only; Test and Evaluation; 30 January 1978. Other requests for this document must be referred to the USAF 414L System Program Office, Electronic Systems Division (AFSC), Hanscom Air Force Base, Massachusetts 01731.

17. DISTRIBUTION STATEMENT (of the abstract entered in Block 20, if different from report)

18. SUPPLEMENTARY NOTES Semiannual Technical Reports 1 through 8 for Contract N00014-70-C-0413 report on tasks completed under ARPA Order 1656, while Semiannual Technical Reports 9 and 10 discuss tasks undertaken on the same contract with ESD sponsorship. The present report was prepared under Contract N00014-75-C-0930, the continuation of Contract N00014-70-C-0413.

19. KEY WORDS (Continue on reverse side if necessary and identify by block number)

Adaptive-array processing
Adaptive beamforming
Aircraft surveillance
Backscatter sounding
CONUS OTH-B experimental radar system
Detection
HF radar
Interactive displays
Ionospheric propagation
Tracking

20. ABSTRACT (Continue on reverse side if necessary and identify by block number)

This report describes major aspects of the technical support provided by SRI International (formerly Stanford Research Institute) to the Electronic Systems Division (ESD), AFSC, in the development of the CONUS 414L Experimental Radar System (ERS). Areas of investigation covered in detail include propagation management and out-of-beam energy rejection. Discussed also are technical studies initiated in direct response to immediate Air Force interests.

(Continued)

DD FORM 1 JAN 73 1473 EDITION OF 1 NOV 65 IS OBSOLETE

UNCLASSIFIED

SECURITY CLASSIFICATION OF THIS PAGE (When Data Entered)

410 281 JOB

UNCLASSIFIED

SECURITY CLASSIFICATION OF THIS PAGE (When Data Entered)

19. KEY WORDS (Continued)

20 ABSTRACT (Continued)

In achieving and confirming the findings, extensive use was made of the Wide Aperture Research Facility (WARF) and its existing over-the-horizon backscatter (OTH-B) HF radar. WARF is an SRI-operated, ESD/ONR-sponsored facility capable of simulating ESD's ERS operations in almost all respects, although on a smaller operating scale.

CONTENTS

LIST OF ILLUSTRATIONS vii

LIST OF TABLES ix

I INTRODUCTION AND SUMMARY. 1

II STATUS OF PRINCIPAL TECHNICAL EFFORTS 7

A. Subclutter Visibility Measurements 7

B. Radio Frequency Interference 11

1. The Bias-Removal Interference-Suppression Algorithm (BRISA) 12
2. A Short Description of BRISA. 13
3. A Test of BRISA 16
4. Discussion. 20

C. Noise Model and Display Evaluation 21

1. A Test of Model Realism 21
2. Display Sensitivity 24

D. Generalized Sidelobe Canceller 31

E. Spread Clutter Effects on Adaptive Beamformers 38

F. Mis-Steered Transmitter Beam 39

III CONSULTING ACTIVITIES 45

APPENDICES

A ARCHITECTURE FOR A HARDWARE BEAMFORMER 47

B GENERALIZED SIDELOBE-CANCELLER SYSTEM-MULTIPLIERS. . . . 53

REFERENCES 57

DISTRIBUTION LIST. 59

ILLUSTRATIONS

1	Subclutter Visibility for 250-nmi Barrier	9
2	Variation in Time Delay (Slant Range) to Nearer Boundary of 250-nmi Barrier	10
3	Optimum Frequency for 250-nmi Barrier	11
4	An Example of Interference Suppression Using BRISA	12
5	Doppler Spectra and Signal Variation for a Radar Dwell	15
6	Radar Data (with Targets and RFI) Processed Using ERS Normalization	17
7	Radar Data (with Targets and RFI) Processed Using BRISA	18
8	Target SNR vs Time	19
9	Distribution of Signal-to-Noise Ratios	19
10	Range (Nested Doppler)-vs-Time--WARF Data	22
11	Range (Nested Doppler)-vs-Time--Simulated Data	23
12(a)	Range (Nested Doppler)-vs-Time Format--Simulated Data with 8-s Refresh	25
12(b)	Traffic Template for Figure 12(a)	26
13(a)	Range (Nested Doppler)-vs-Time Format--Simulated Data with 8-s Refresh	27
13(b)	Traffic Template for Figure 13(a)	28
14(a)	Range (Nested Doppler)-vs-Time Format--Simulated Data with 8-s Refresh	29
14(b)	Traffic Template for Figure 14(a)	30
15	Generalized Sidelobe Canceller	32
16	Performance of GSC Processor (Frost Algorithm) Against Simulated Signals	36
17	Performance of GSC Processor (Griffiths Algorithm) Against Simulated Signals	37
18	Geometry of Transmitter Mis-Steering Test (not to scale)	40
19	Typical Doppler Power Spectra Observed During the Clutter-Cancellation Test of the GSC Processor	41
A-1	Architecture for an Operational Generalized Sidelobe Canceller	50

TABLES

1	Data Summary for Mis-Steered Transmitter Beam Test.	42
B-1	Circuit Costs	56
B-2	Multiplier Performance.	56

I INTRODUCTION AND SUMMARY

This semiannual technical report describes major aspects of the technical support provided by SRI International* to the Electronic Systems Division (ESD), Air Force Systems Command (AFSC), in the development of the CONUS 414L Experimental Radar System (ERS). The work was performed during the period 1 January through 30 June 1977 under Contract N00014-75-C-0930.† To resolve questions pertinent to risk areas in the ERS, SRI has used the Wide Aperture Research Facility (WARF), an existing over-the-horizon backscatter (OTH-B) HF radar. WARF is an SRI-operated, ESD/ONR-sponsored facility capable of simulating ESD's ERS functions in almost all respects, although on a smaller scale. WARF serves as a test-bed for newly developed OTH-B techniques related to the ERS procurement.

The CONUS 414L Experimental Radar System currently being procured is an over-the-horizon HF backscatter radar designed to detect and track all aircraft passing through the North Atlantic air corridors. Requirements for extended range coverage and broad azimuthal sectors dictate the use of a large energy product, and time-sequential range-changing and azimuth-scanning capability. Normal commercial traffic passing through the radar coverage requires that a large number of tracks be maintainable at all times. Facilities for real-time correlation and identification will be implemented at the radar receive site. The azimuth sidelobe levels of the receive antenna system are presently specified at -50 dB as a means for assuring ERS operation near the auroral zone without

---

*Formerly Stanford Research Institute.

†Contract N00014-75-C-0930 was issued by the Office of Naval Research as a continuation of Contract N00014-70-C-0413. Its sponsors (each for different aspects of OTH technology) are ESD (AFSC), ONR, and ARPA. The Scientific Officer for the overall contract is Mr. John J. Kane, ONR [Code 461(FP)], telephone (202) 692-4203.

reception of intolerable levels of auroral clutter. The ERS system performance test is currently scheduled to begin in FY80. Conclusions drawn from the ERS design will support the transition to the fully operational radar system (RS).

During this reporting period, work on the project at SRI has been directed toward the following:

- Use of a subclutter visibility (SCV) measurement technique for collecting round-the-clock data on potential radar sensitivity for any available choice of radar parameters.
- Development of a technique for the suppression of radio frequency interference (RFI).
- Implementation of a model for OTH-B radar data to test the sensitivity of the ERS display of Doppler (nested range) vs. time and its detection/tracking (D/T) systems.
- Development of a generalized sidelobe canceller (GSC) beamforming processor.
- Study of spread-clutter effects on adaptive beamformers and preliminary testing of the GSC against azimuthally spread clutter generated by mis-steering the WARF transmit beam.
- Investigation of architectures for hardware implementation of an adaptive beamforming processor like the GSC.
- Provision of direct support to the ESD 414L SPO through special on-request studies, visits, and consultations concerning the ERS.

The status of each effort is briefly summarized below.

The round-the-clock measurements involve a year-long data collection effort now near its midpoint. Analysis of the soundings has been made with the recognition that the current operating concept for the ERS will provide a single radar fence (barrier) that moves in range as propagation conditions change. First analyses indicate that:

- Azimuthal variations of SCV are small over most of the diurnal cycle, so the best operating parameters for an azimuth-scanning radar may be obtained by sampling only a few azimuthal bearings. The major exception to this result will occur at ERS during certain periods of auroral activity when it is expected that one edge of the azimuthal coverage sector will be up against the edge of intense auroral scatter.
- Usable barrier depth is limited to ranges less than 500 nmi. Two 24-hour tests show that the outer half of the 500-nmi barrier is

substantially less sensitive (often as much as 20 dB) than the inner half. This state of affairs should generally hold for the ERS environment as well.

- Predicted nighttime radar sensitivities are higher than those measured at WARF during 24-hour aircraft surveillance tests. A number of explanations are possible, one of which is that there has been a reduction at the radar of atmospheric and man-made noise originating from the east. This reduction is most likely the result of installation of 256 twin-whip endfire receiving pairs (TWERP) in place of the 256 single vertical whips used during the 24-hour aircraft surveillance tests.
- Large and frequent inward or outward movements of the barrier will be necessary if higher radar sensitivity is to be maintained. A tradeoff between sensitivity and barrier movements will be required to avoid missing targets through discontinuities in barrier coverage.
- Existing off-line algorithms designed as automatic aids for selecting the best radar operating parameters perform consistently well, and could become valuable aids in on-line propagation management, even though they do not currently account for multipath, auroral clutter, or frequent large barrier movements.

RFI is an anticipated problem for the ERS. MITRE expects a typical RFI environment of several (3 to 5) carrier sources, each having approximately a 20-dB SNR and leading to SNR degradations of 20 dB for several target speeds. An SRI-developed RFI-suppression algorithm known as BRISA* can be applied directly to scalar amplitude data after coherent processing to reduce or eliminate almost all RFI signal energy. Basically, BRISA seeks by efficient computer processing to eliminate the bias introduced by the constant level of RFI containing carrier components. The expected 20-dB SNR degradations for several target speeds should be reducible to about 3 dB for each of these speeds through application of BRISA. Coupling of BRISA to the frequency-stepping technique proposed by MITRE should significantly improve ERS performance, especially in the typical nighttime environment. In this report we demonstrate the present capabilities of BRISA in processing WARF data.

---

*BRISA: Bias-Removal Interference-Suppression Algorithm.

An SRI-developed analytical model that simulates radar target and noise data provides a controlled environment for the test, evaluation, and comparison of the WARF animated display system and the ERS gray-scale display format. The model provides for dwell-to-dwell SNR fluctuations, target signature changes including range and/or Doppler spreading of target signatures, and randomly occurring meteors at a prespecified expected rate of occurrence. Not included are long-term fading over many dwells and signature variation within an established track.

An initial test of the analytical model was directed toward determining the detection sensitivity of the ERS display. Earlier tests done elsewhere evaluated display sensitivity with nonfluctuating CW signals in noise and used progressively stepped SNR levels. The model tests at SRI sought to reduce the element of bias introduced by the monotonic steps of the earlier tests. A display of range (nested Doppler) versus time containing targets of 0 to 20 dB SNR was generated. Our analysis of the tracks within the simulated ERS display data yields an estimated display sensitivity of between 6 and 9 dB as the SNR required to obtain a 50% detection rate. This figure is representative of manual detection results; use of the SEDAT* algorithm should lower this threshold somewhat. In any event, the manual detection threshold as determined by this model of the ERS display is several dB higher than that determined by the tests involving nonfluctuating CW signals.

The University of Colorado under subcontract to SRI has developed a new adaptive noise-cancelling scheme referred to as a Generalized Sidelobe Canceller (GSC). A most promising aspect of this processor structure is that it permits the realization of a fairly general class of adaptive beamforming algorithms with a single unifying analytical approach. A version of this processor has been implemented in software at SRI for off-line processing of WARF data and for preliminary performance evaluation. The GSC is important because with further development it could

---

*SEDAT: Sequential Detection and Tracking.

provide a fallback method for rejection of auroral clutter at the ERS site or for the eventual R3.

Application of adaptive beamforming techniques to HF radar is attractive because of their potential for rejecting spread-azimuth and spread-Doppler clutter such as that produced by scattering from auroral irregularities. A number of alternatives have been considered for using the WARF adaptive beamforming capabilities to test methods of rejecting spread-azimuth interference on an experimental basis (in contrast to computer simulation studies that cannot reasonably account for various aspects of the HF environment and the constraints on HF equipment). Options include generation of azimuthal and Doppler spreading by (1) using a separate transmitter to transmit a 2-hop signal that is received as clutter in the sidelobes of the receive array, (2) mis-steering the WARF transmit beam to generate a clutter distribution with significant out-of-beam components, (3) collection of scatter from spread-F ionization, or (4) use of ionospheric heating to generate field-aligned irregularities similar to those found in auroral regions. Anticipated frequency management difficulties have caused us to reject the separate transmitter approach. The mis-steering option has been tried and is discussed in this report. Observations of spread clutter due to ionospheric heater-induced irregularities may be carried out in FY78.

In a preliminary test of the capability of the GSC beamformer to reject spread clutter, the WARF transmit beam was steered away from the desired target (the Los Lunas, New Mexico repeater) so as to introduce substantial ground clutter in the sidelobe angles of the receive beam (Option 2 in the previous paragraph). In brief, the average signal-to-clutter ratio (SCR) improvement with the adaptive beamformer, compared to a conventional beamformer, operating in a clutter environment was measured at 8 dB with beam alignment and 11 dB with beam misalignment. The tests clearly demonstrate that appreciable cancellation of clutter spread in azimuth is achievable by an adaptive technique.

As a part of the ongoing analysis of adaptive beamformers at SRI, a study has been initiated to define how an on-line beamformer might eventually be best implemented. The GSC structure was used as a candidate system to obtain a measure of cost, speed, and performance of such a device when integrated into the operation of an OTH radar. The GSC structure led to a design for a multiplier-oriented processor which, considering the complexity of operations and the desire to modify the GSC algorithm in real time, suggested a microprocessor-based controll' if the des_gn is ultimately executed in hardware devices. The MOS class of microprocessors would be too slow, having instruction times of at least 1 μs, so a bipolar microprocessor slice or a microprogram sequencer might be viable alternatives. System architecture and some aspects of hardware realization are discussed in Appendices A and B.

Finally, with respect to the provision of direct support to the ESD 414L SPO, SRI participated in conversion of the PRS concept to the ERS; originated approximately 200 hours of sounding transmissions for reception by RADC; developed preliminary design and cost estimates for transponders usable in the ERS coverage; and developed a technical concept for augmenting the ERS with an independently operated environmental assessment system, a minicomputer-based system designed to improve ionospheric propagation management capabilities at the ERS.

II STATUS OF PRINCIPAL TECHNICAL EFFORTS

A. Subclutter Visibility Measurements

SRI has developed a method of measuring SCV from the widesweep backscatter sounder (WSBS) used for propagation management. This method has the advantage that radar sensitivity can be inferred for all possible range gates and frequencies, not just those currently used by the radar. On-line use of this measurement technique during a WARF 24-hour aircraft-tracking test in August 1975[1*] demonstrated its ability for optimizing the selection of radar operating parameters.

Because this WSBS-SCV technique is a direct measure of potential radar sensitivity for all ranges and frequencies it is a useful tool for characterizing potential radar performance. Such information could be valuable for determining ERS performance and developing procedures for propagation management. For these reasons SRI has undertaken a one-year experimental program designed to collect 24 hours of WSBS-SCV data approximately once each month. In this program a sounding is taken every 5 minutes. Three azimuth directions spaced 15° apart are sounded sequentially, achieving a revisit at each azimuth every 15 minutes. Each sounding covers from 6 to 27 MHz in frequency and from 0 to 24 ms in time delay.

Existing WARF computation facilities are inadequate to process and display these results in real time. A data-collection program was devised that collects the raw data and does sufficient real-time processing to reduce the amount of data to within manageable limits. The resulting data are recorded on digital magnetic tape for later processing at SRI Menlo Park.

During this reporting period, soundings from five continuous 24-hour periods were recorded. Initial analysis was directed toward assessing

---

*References are listed at the end of this report.

the potential performance of an OTH radar operating in a three-range-gate, three-frequency format such as that originally proposed for the Prototype Radar System (PRS). For each of these range gates the computer analysis involved a search to locate the frequency that maximized average SCV. These frequencies and the resulting SCVs were then plotted versus time. In accordance with a change in the proposed radar system design, this analysis was later repeated with the restriction that only the A, C, and E high-frequency radio bands were available for radar use.

In mid-February 1977 a design revision of the 414L program changed the PRS to an Experimental Radar System (ERS). The new radar operating concept consists of a single radar fence (barrier) that moves in range as propagation conditions change. SRI's SCV soundings were reanalyzed to reflect this change in operation concept. Each sounding was searched in frequency and time-delay to maximize the average SCV over the range extent of the barrier. Barrier depths of 500 and 250 nmi were chosen for this analysis. Figures 1, 2, and 3, respectively, plot SCV, time delay (slant range), and frequency versus time for the 24-hour period starting on 12 April 1977. A 250-nmi barrier was selected in the analysis used to make these plots.

Thus far, analysis of the soundings has produced the following findings:

(1) Azimuthal variations are small. Based on analysis of two 24-hour tests, it appears that differences in operating parameters selected independently for the three azimuths monitored were small over most of the diurnal cycle. Thus it may not be difficult to determine the best operating parameters for an azimuth-scanning radar by sampling only a few azimuth bearings.

(2) Usable barrier depth is limited to ranges less than 500 nmi. It appears that radar sensitivity for a single radio frequency decreases rapidly with range, once past the skip distance. Based on two 24-hour tests, a comparison of average SCV for the 250- and 500-nmi barriers shows that the outer half of the 500-nmi barrier is substantially less sensitive (often as much as 20 dB) than the inner half. For this reason we have chosen to use the 250-nmi barrier as the basis for further analysis.

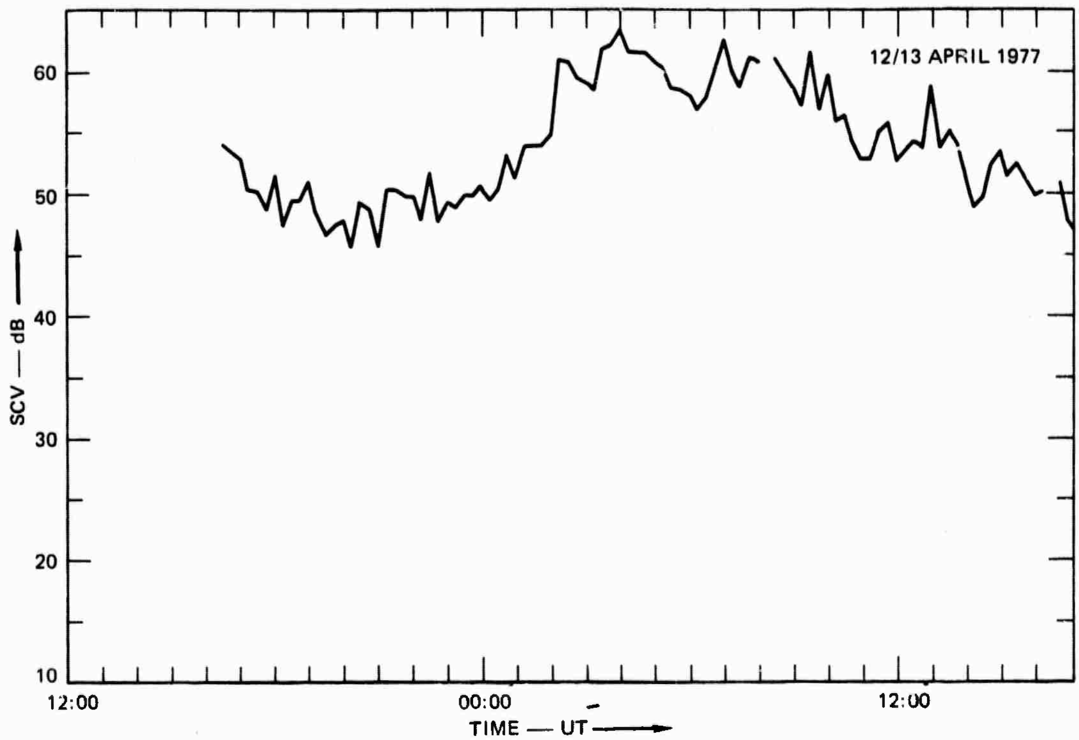

FIGURE 1 SUBCLUTTER VISIBILITY FOR 250-nmi BARRIER

(3) Nighttime sensitivity appears better than expected. As seen in Figure 2, the predicted nighttime SCVs are quite high, significantly higher than those measured from the radar directly during 24-hour aircraft surveillance tests at WARF. It is not yet known whether this effect is real or due to complexities in the measurement of SCV. Possible explanations include computational underflow; algorithm difficulties brought about by the nighttime RFI environment; the presence of spread-F (which could reduce radar sensitivity without affecting sounder-inferred sensitivity); or, finally, the use in the WARF receiving array of TWERPS* instead of single array elements (which reduces atmospheric and man-made noise originating from the east). A 24-hour aircraft surveillance test planned for FY78 will yield

---

*TWERP: Twin-whip endfire receiving pair. Use of 256 TWERP elements in the WARF receiving array yields a switchable cardiod pattern designed to enhance reception from the east or the west, as selected by the site operators.

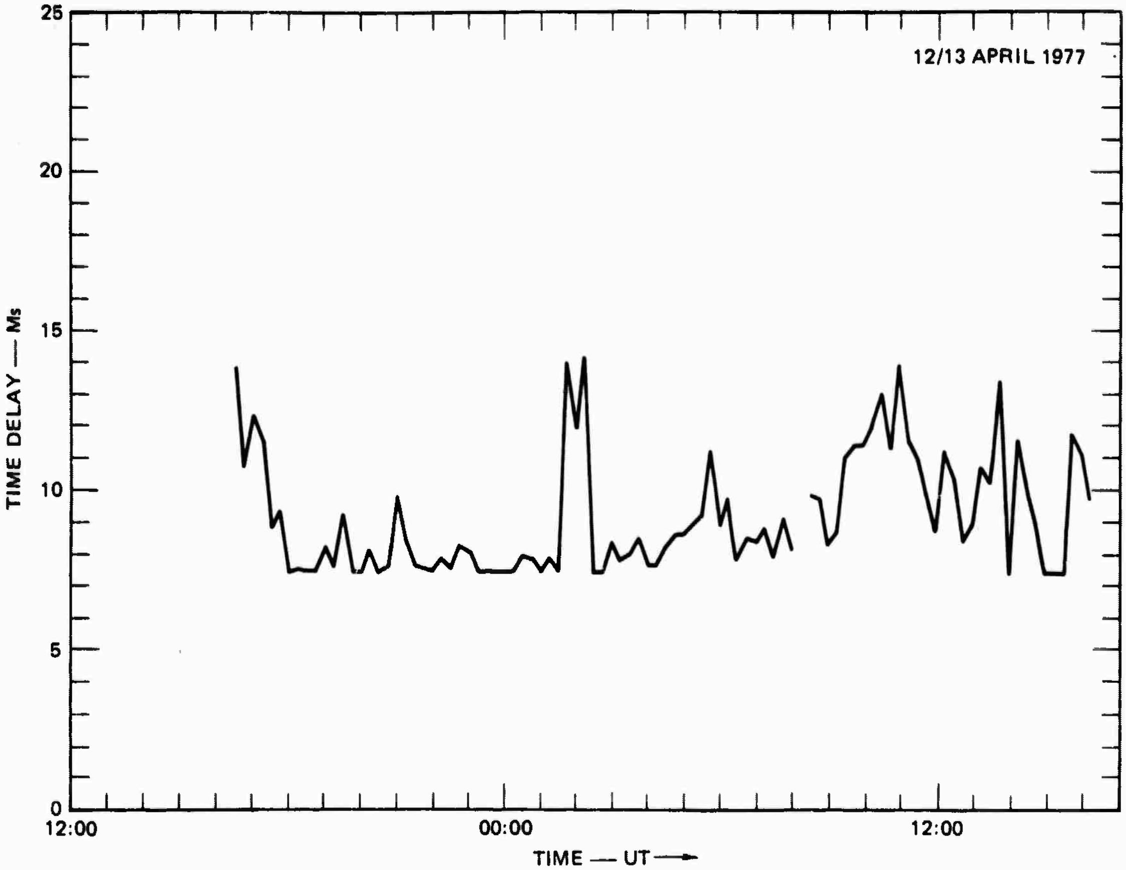

FIGURE 2 VARIATION IN TIME DELAY (slant range) TO NEARER BOUNDARY OF 250-nmi BARRIER

additional information on the contribution of TWERPS to higher SCV levels.

(4) Strict maximization of SCV causes unwanted gaps in radar coverage. The analysis programs choose an operating frequency and range gate that maximizes SCV. As seen in Figure 2, this criterion can result in large fluctuations of the barrier position. To avoid missing targets through discontinuities in barrier coverage, it is desirable to maintain a fixed barrier position or one that changes only in small increments. Thus it appears that a tradeoff is often necessary between sensitivity and amount of barrier movement.

(5) Automatic aids for propagation management appear achievable. The programs developed for off-line analysis of SCV soundings use automatic methods for selecting operating parameters. Currently these algorithms do not

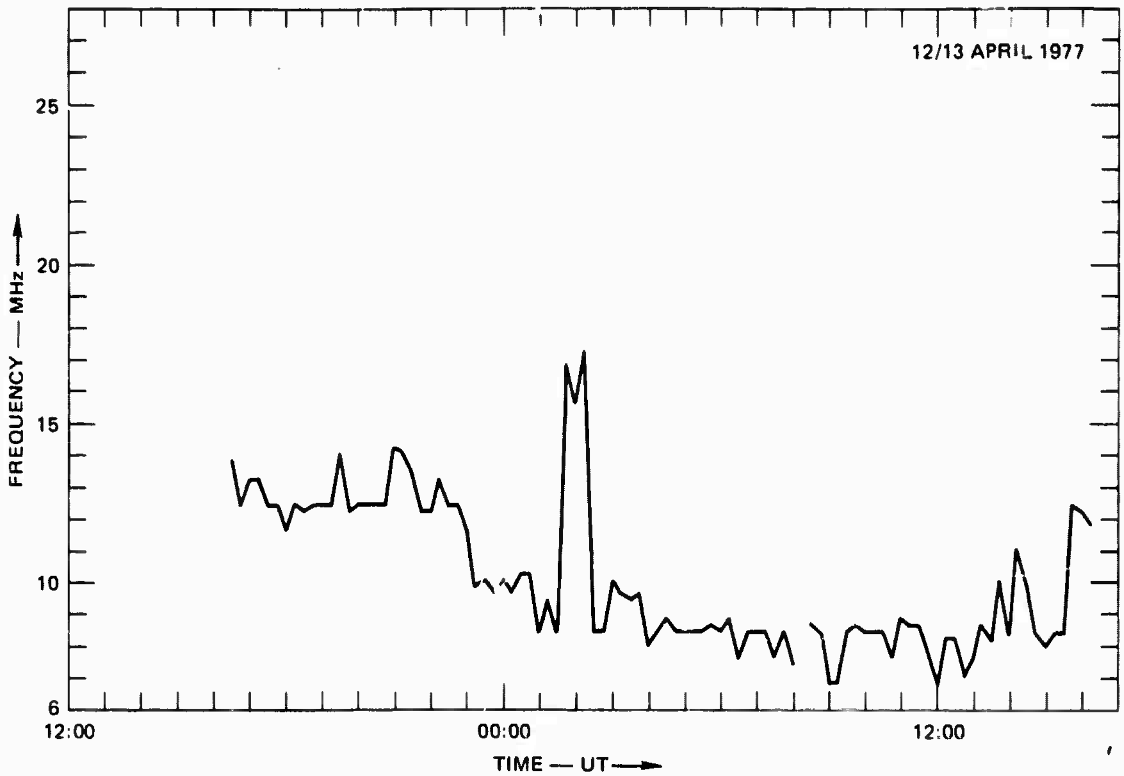

FIGURE 3 OPTIMUM FREQUENCY FOR 250-nmi BARRIER

consider multipath, auroral clutter, or frequent large barrier movements. Nonetheless, the algorithms do perform consistently well in selecting the best operating parameters, as determined by post-operating analysis. With further modification, the algorithms could become valuable aids in on-line propagation management.

Continuation of the collection of round-the-clock SCV measurments is planned for the next six months. A technical report describing the sounding system, methods of analysis, and early results will be issued.

B. Radio Frequency Interference

To maximize sensitivity of an OTH radar it is essential to avoid or suppress interfering signals caused by other radio transmissions. In normal operation of an OTH radar all possible measures should be taken to select frequencies that are free of interference. Unfortunately, at times (particularly winter nights) it will be impossible to avoid interference entirely, and thus RFI suppression techniques will be necessary to maintain radar sensitivity. Also, since interference often occurs unexpectedly, use of a RFI suppression algorithm is necessary to maintain operations until a new and better operating frequency can be selected.

The previous semiannual report described work conducted at SRI in the investigation of spectrum-monitoring techniques for RFI avoidance, and in the evaluation of various proposed RFI-suppression techniques. During the period dealt with in the previous report, a promising new approach to RFI suppression was conceived. It has now been developed at SRI, and is called the Bias-Removal Interference-Suppression Algorithm (BRISA). A description of BRISA is presented here, along with some examples demonstrating its ability to remove the deleterious effects of RFI. Perhaps the most remarkable feature of BRISA is the simplicity with which it handles a complex signal environment with only a slight increase in signal-processing requirements.

1. The Bias-Removal Interference-Suppression Algorithm (BRISA)

The most troublesome signal component contained in most interfering radio transmissions is the coherent "carrier." At the output of the radar processor this carrier is compressed in Doppler, thus creating a relatively large interference level that can mask targets at the same Doppler. Cost-effective methods have been developed to spread this type of RFI throughout all Doppler cells and thus minimize the average system degradation. A preferable approach would be to reduce or eliminate the RFI signal energy itself. Methods to do this include adaptive beamforming and compressive filtering. However, these methods are costly in terms of radar processor loading. The algorithm presented here is a relatively simple computation that can eliminate much of the unwanted RFI energy. When used in conjunction with the RFI frequency-stepping techniques, this new algorithm should be able to eliminate most deleterious effects of RFI.

BRISA is applied directly to the scalar amplitude data after coherent processing. Attributes of BRISA include the following:

- Requires only simple computations to be performed on radar data after range/Doppler processing.
- Affects only those Dopplers having range-correlated RFI.
- Does not affect range sidelobes.
- Can suppress RFI energy by 30 dB or more.
- Can suppress multiple carriers simultaneously.
- Can be used in conjunction with phase- or frequency-stepping RFI-spreading techniques.

2. A Short Description of BRISA

The effect of BRISA and the way in which it suppresses interference can best be described with the use of an example. The plots of Figure 4 show the output from a single OTH radar dwell. These data were collected at WARF. A target of opportunity and a controlled RFI source

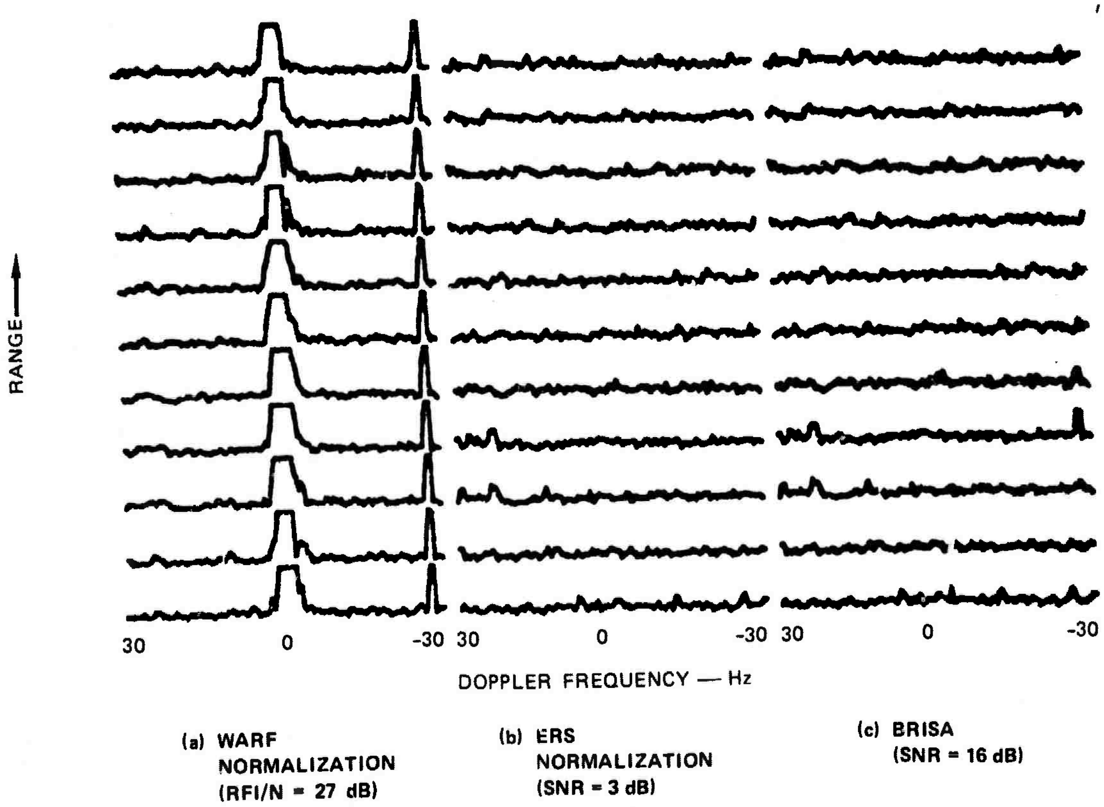

FIGURE 4 AN EXAMPLE OF INTERFERENCE SUPPRESSION USING BRISA

are contained within these data. In each plot, amplitude is plotted versus Doppler for each of 12 range resolution cells. The three plots of Figure 4 each show a different method of data normalization for the same radar dwell.

Figure 4(a) represents the normalization used for the WARF radar detection display. One estimate of noise is made for the radar dwell and all amplitudes are normalized (divided) by this value. Very large signals such as the clutter near zero Doppler and the RFI at -27 Hz are clipped 20 dB above the computed average noise value. This normalization has the disadvantage of presenting a nonuniform background, but this is partially compensated for by the ability to easily detect the presence of RFI energy.

Figure 4(b) represents the normalization planned for use with ERS. For each Doppler (column) an estimate of noise is calculated and amplitudes within each column are then normalized (divided) by the noise value at that Doppler. This normalization has the advantage of whitening the entire display field, but at the cost of suppressing all information on the presence of RFI. While the presence of strong signals such as clutter and RFI have been eliminated from the display, this normalization of course does not improve target detectability at the clutter and RFI Dopplers.

In Figure 4(c) BRISA has been applied to the data with the result that a target echo of approximately 16 dB signal-to-noise ratio (SNR) is now visible at the RFI Doppler frequency. To achieve this target detection, BRISA has taken advantage of the fact that while the RFI carrier adds extra power at a particular Doppler, it adds the <u>same</u> amount of power to all range bins at that Doppler. Thus, while the average amplitude of each range bin can be greatly increased by an RFI signal, the standard deviation (σ) of these range bins is only slightly altered. Since detection is really limited by noise fluctuation, (proportional to σ)* and not

---

*For Rayleigh-distributed amplitudes (a good approximation of the noise and, to a lesser extent, clutter amplitudes) the mean (m) is linearly proportional to the standard deviation (σ), and division by the mean is therefore appropriate. For RFI (which is not Rayleigh distributed) the mean can be very large while the standard deviation remains small. Hence, division by the mean is not the best method of optimizing SNR.

by its average value, a target is detectable despite the presence of this RFI.

BRISA seeks to eliminate, before normalization, the bias introduced by the constant level of RFI. The way the bias is removed can be demonstrated by the example of Figure 5. Here the radar dwell of Figure 5 has been reprocessed. For each Doppler resolution cell in Figure 5(a) the rms amplitude of the 12 range cells is plotted on a logarithmic scale. Also plotted is the peak amplitude of the 12 range cells. Noise, clutter, and RFI are distributed in range, so the rms plot is appropriate to estimate their strength. On the other hand, a target is confined in range and here the peak plot is appropriate for measuring its strength. Hence, both rms and peak plots are needed to determine such quantities as SNR and signal-to-interference ratio. In Figure 5(b) the ratio of the

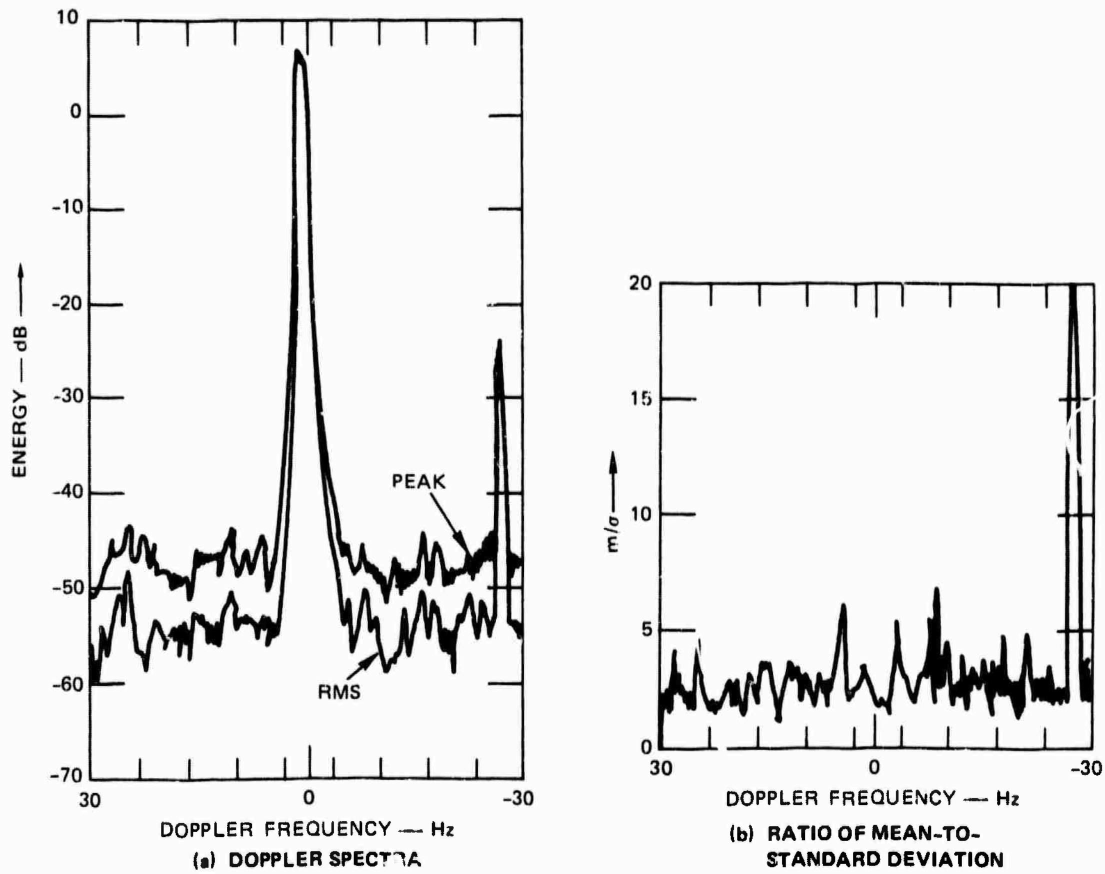

FIGURE 5 DOPPLER SPECTRA AND SIGNAL VARIATION FOR A RADAR DWELL

mean (m) to the standard deviation (σ) of the amplitudes for the twelve ranges in each Doppler resolution cell has been plotted. For Rayleigh-distributed values (such as noise and, to a lesser degree, clutter) the ratio of m/σ should be about 2. It can be seen from Figure 5(b) that this ratio holds approximately true for Dopplers having both clutter and noise. For Dopplers containing RFI, however, the m/σ ratio sharply increases.

The BRISA algorithm calculates the m/σ ratio for each Doppler. For those Dopplers where m/σ is below a threshold (say, 5) the algorithm presumes that only noise or clutter is present, and the standard ERS normalization is performed. For Dopplers with m/σ greater than 5, BRISA first subtracts the mean amplitude at that Doppler (m) from all amplitudes at that Doppler. Since this produces both positive and negative values (a strong target might have a large negative value, depending upon its phase relationship to the RFI), the absolute value of each amplitude is taken after subtraction of the mean. Finally, the standard ERS normalization is then performed. The results of this process are shown in Figure 4(c).

3. A Test of BRISA

For the purpose of this brief description it is appropriate to provide an example of the performance of BRISA. Radar data were collected using the WARF radar. During data recording, a local RFI source (with approximately 25 dB SNR) was switched on and its frequency was controlled to place the RFI on the radar output at the same Doppler as an observed target of opportunity. These data were recorded to be used in later analysis of different normalization techniques. Figure 6 displays a 15-minute data sequence in the range-versus-time display (nested Doppler) format to be used at the ERS. Standard ERS normalization has been performed.

In Figure 7 the same data have been reprocessed using BRISA. The increase in track detectability is apparent. In Figure 8 the target's SNR versus time is plotted for the standard ERS normalization (Figure 6) and for BRISA normalization (Figure 7). Figure 9 replots the data of Figure 8 in histogram fashion. These results demonstrate that application

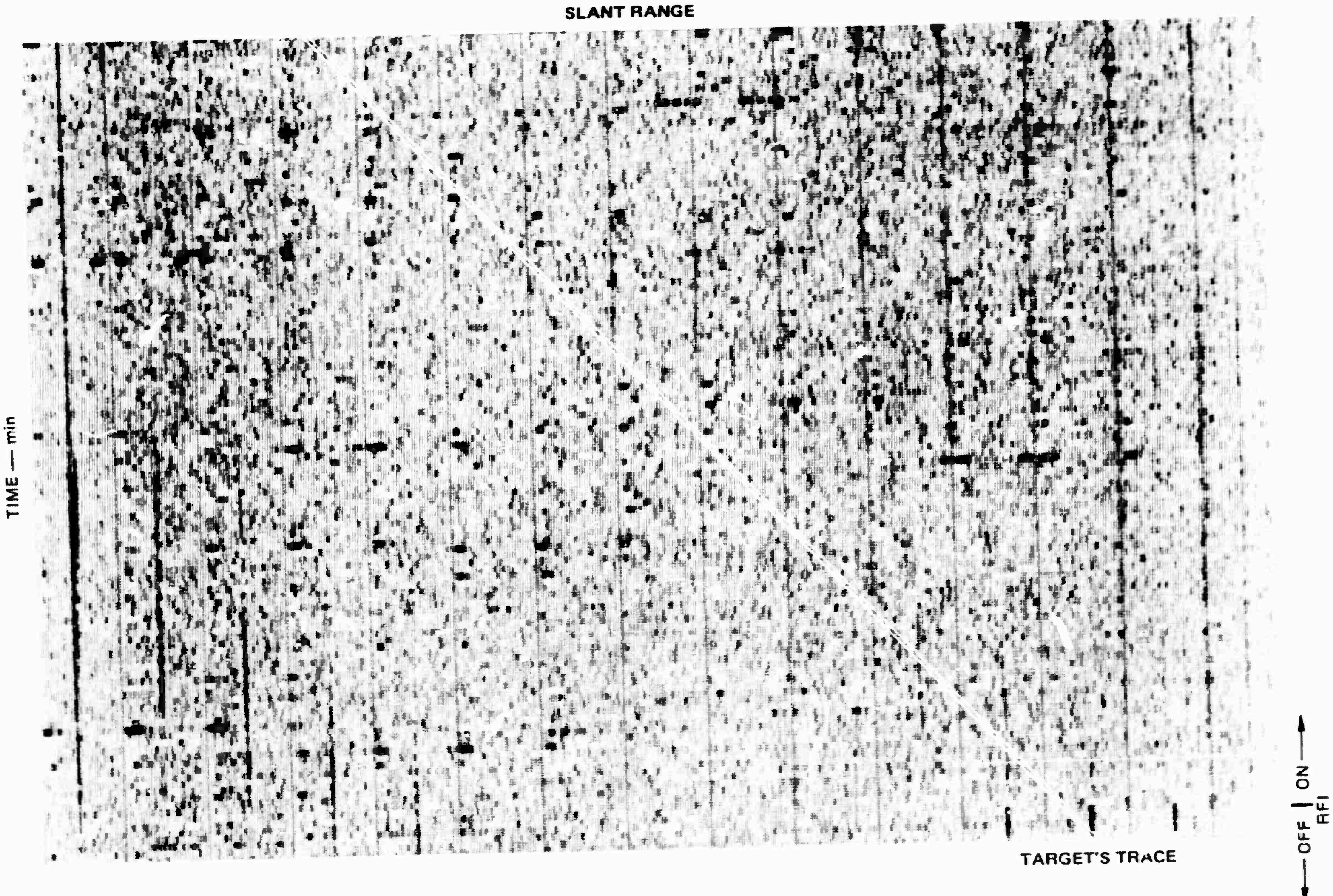

FIGURE 6 RADAR DATA (with targets and RFI) PROCESSED USING ERS NORMALIZATION

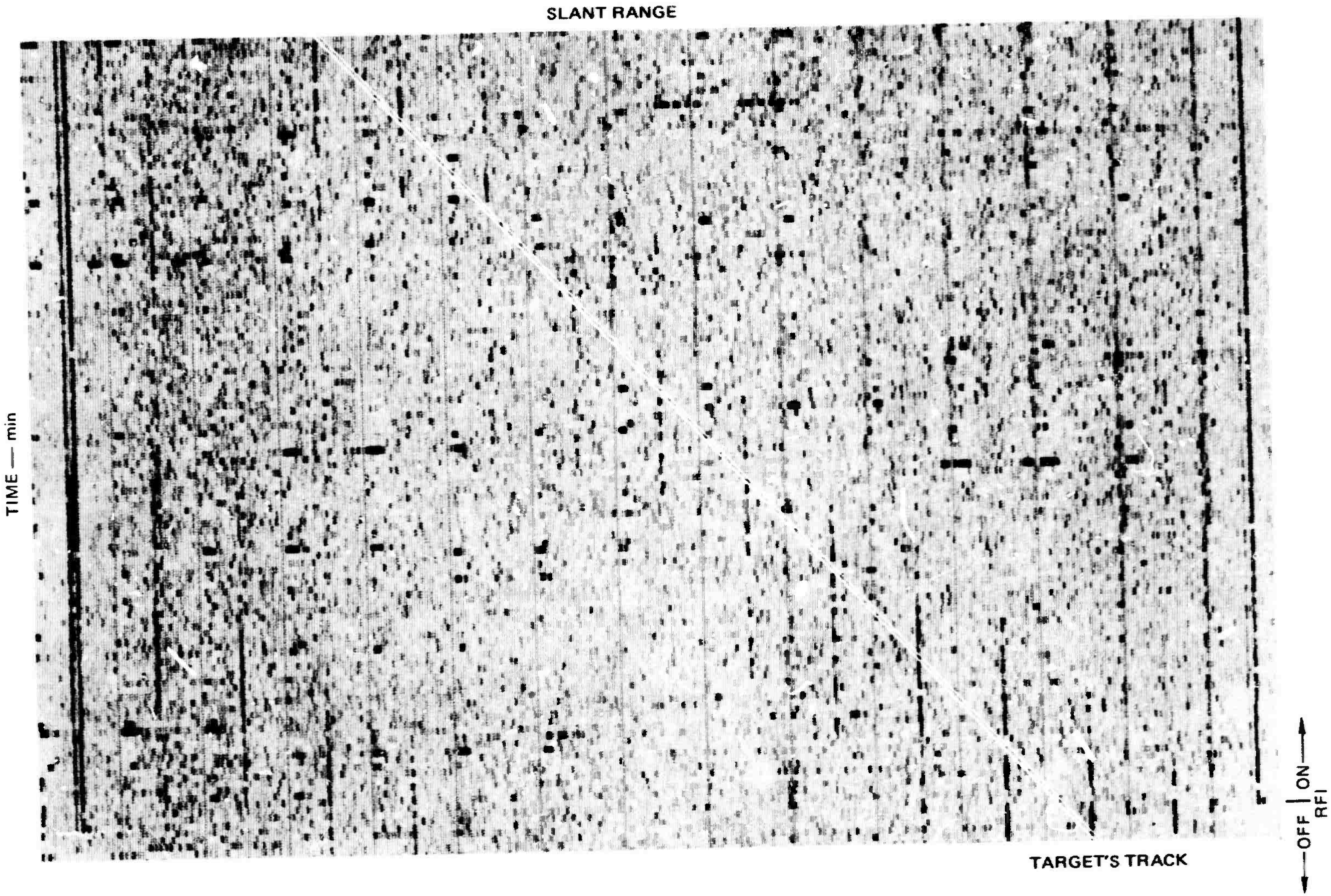

FIGURE 7 RADAR DATA (with targets and RFI) PROCESSED USING BRISA

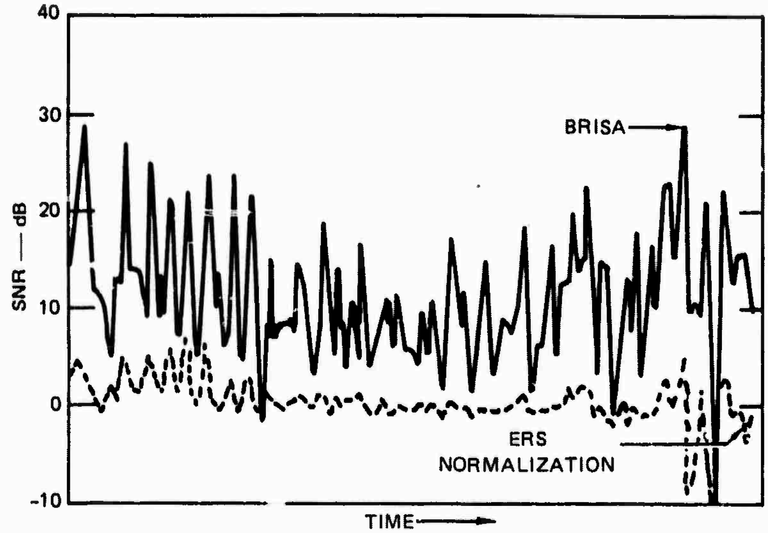

FIGURE 8 TARGET SNR vs TIME

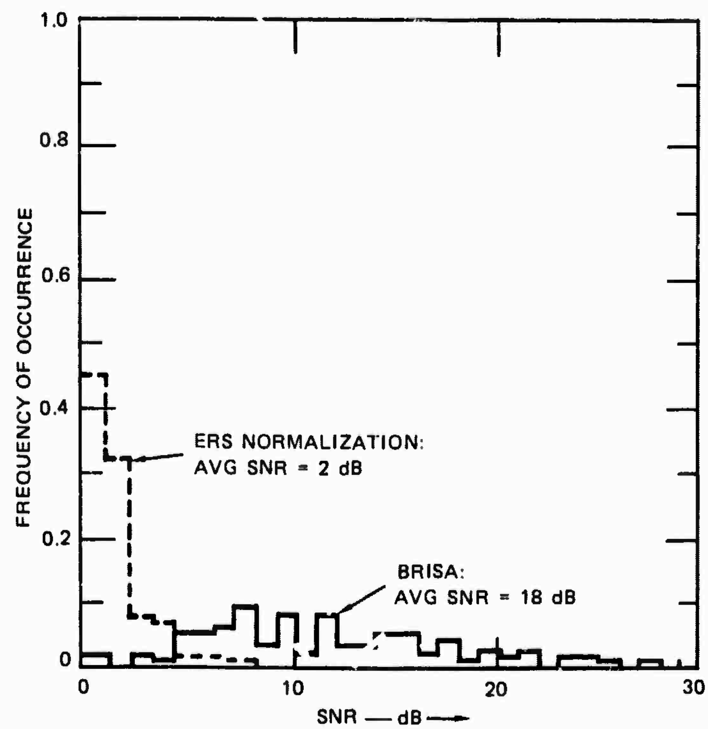

FIGURE 9 DISTRIBUTION OF SIGNAL-TO-NOISE RATIOS

of BRISA can make significant difference for target detectability in the presence of RFI.

4. Discussion

Several observations made during the development of BRISA are listed below:

- The amount of RFI that can be suppressed by BRISA is limited by the accuracy with which the receiver passband is known. (WARF results indicate that 30-dB suppression is easily achievable.)
- Degradation of the algorithm performance was observed as the RFI source was positioned toward the edges of swept bandwidth. (The controlled RFI source used in the data sequence shown above was placed approximately at the middle of the swept bandwidth. Over 20 dB suppression was achieved for more than 50% of the swept bandwidth.)
- BRISA may need modification for use with radar waveform parameters that produce a high RFI time-bandwidth product (radar processor IF bandwidth times the length of time the RFI is in that bandwidth each waveform sweep). The parameters used in collecting the data of Figures 6 and 7 have an RFI time-bandwidth product of 1. However, no noticeable degradation in suppression performance was observed when a time-bandwidth product of 10 was used.
- BRISA worked as well on real RFI sources (i.e., skywave signals) as it did on the local RFI source used in the above measurements.
- BRISA can potentially work on all components of RFI. BRISA performance is not limited by a spread-Doppler RFI source as long as its spectrum remains constant as the RFI is swept through the receiver passband.

In summary, BRISA promises to be an attractive solution to the RFI problem foreseen for the ERS. As has been pointed out by MITRE, the typical RFI environment will consist of several (3 to 5) carrier sources, each having approximately a 20-dB SNR. With the current normalization, such RFI will result in SNR degradations of 20 dB for several target speeds. Application of BRISA could reduce this degradation to less than 3 dB for each of these speeds. Coupled with the frequency-stepping technique proposed by MITRE, application of BRISA should significantly improve ERS performance during the difficult nighttime RFI environment.

C. Noise Model and Display Evaluation

In 1976 SRI developed an analytical model that simulates OTH-radar target and noise data.[2] During the current reporting period this data model was implemented on the Hewlett-Packard 2100 minicomputer facility located at the Remote Measurements Laboratory of SRI. This facility has the capability of generating both the WARF animated display and the ERS gray-scale display. Thus, computer implementation of the data model provides a controlled environment for the test, evaluation, and comparison of these display formats.

1. A Test of Model Realism

The analytical data model was developed for the purpose of providing realistic targets and noise. To accomplish this, the model was based on target and noise statistics extracted from real OTH-radar data collected at WARF. To determine how well the model simulates actual OTH radar data, a test run was conducted to recreate a specific target track obtained at WARF. Figure 10 presents a range (with nested Doppler)-vs-time display of WARF radar data showing two aircraft tracks. Figure 11 presents a recreation of Figure 10 using the OTH data model. The Dopplers of the recreated tracks do not precisely coincide with those of the original tracks because, for simplicity, the model assumes an operating frequency of 15 MHz while the data were actually collected at a higher frequency. Other noticeable differences include:

- Target fading--Dwell-to-dwell SNR fluctuations are part of the data model. However, long-term fading (over several dwells) such as can be seen in Figure 11 is not included in the model.
- Target signature changes--A target signature function is included in the model to simulate range and/or Doppler spreading of targets. This signature function is restricted to remain constant during the progress of each track. However, in the case of actual targets, signatures can change as the target proceeds (e.g., range spreading decreases as targets increase in range in Figure 10).
- Meteors--The model has the capability of including randomly occurring meteors at an expected average rate of occurrence. (Meteors appear as the small dark rectangles

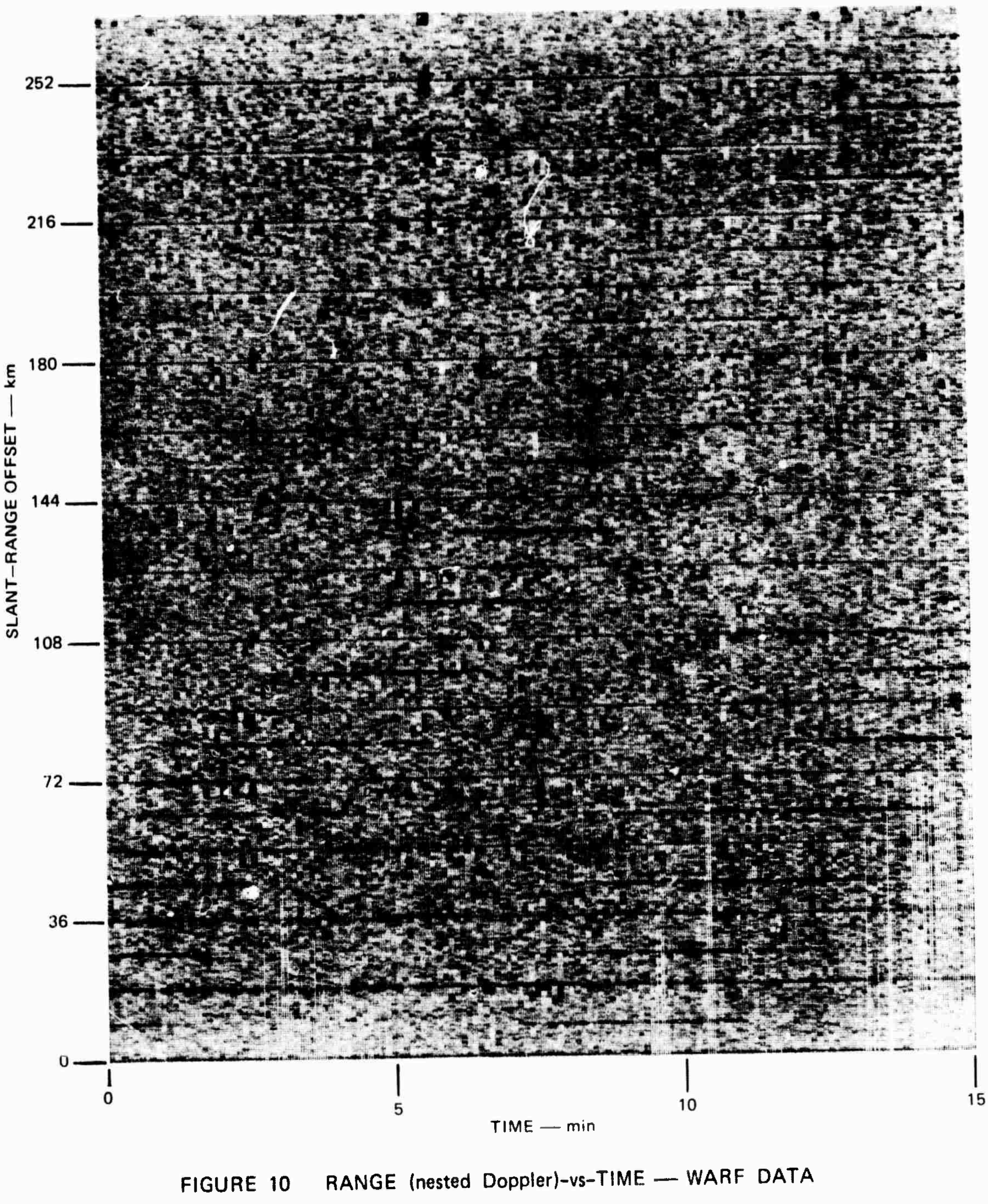

FIGURE 10 RANGE (nested Doppler)-vs-TIME — WARF DATA

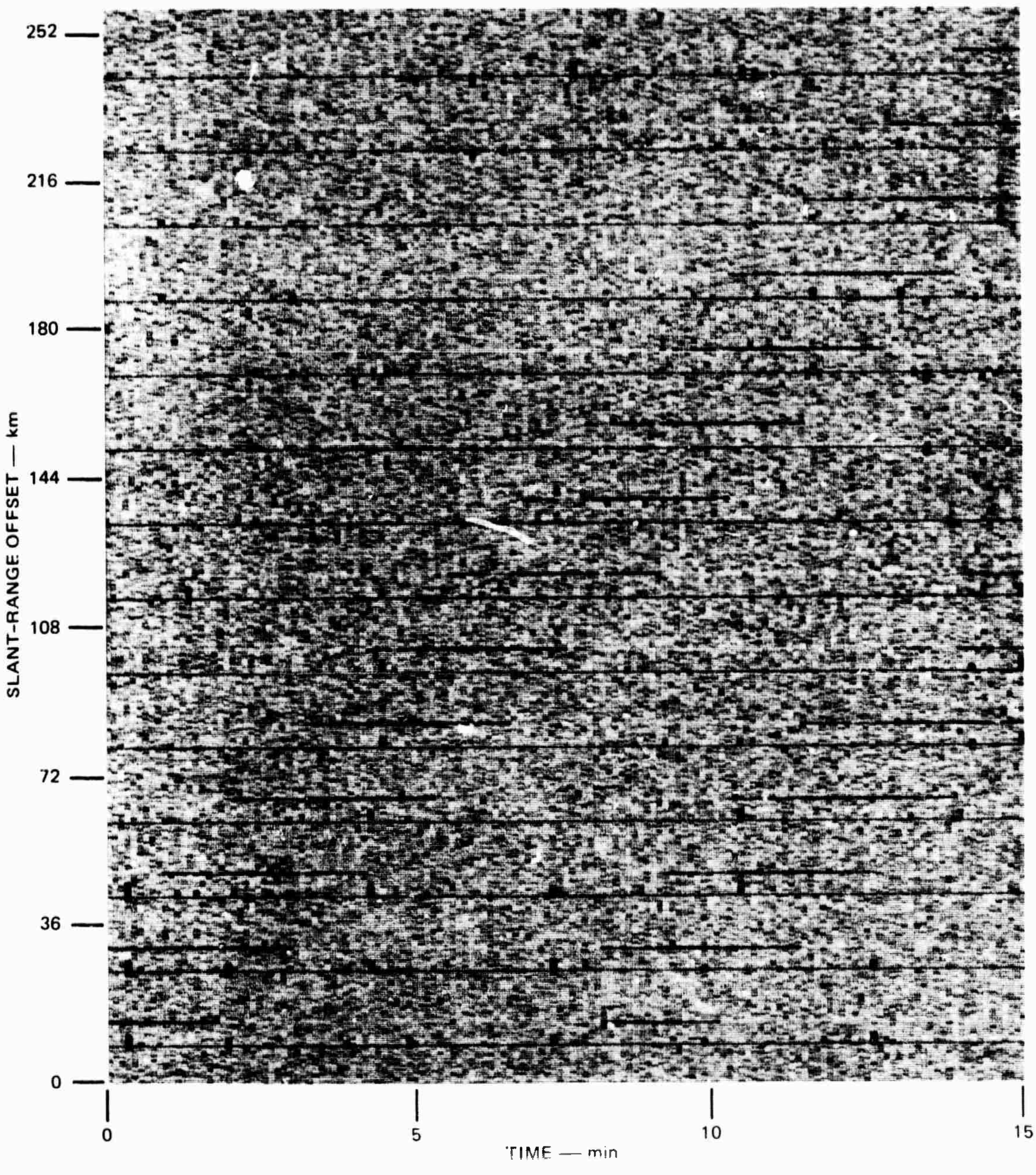

FIGURE 11 RANGE (nested Doppler)-vs-TIME — SIMULATED DATA

on the displays.) However, a comparison of Figures 10 and 11 indicates that the signature function and amplitude distribution function used to simulate meteors could be improved.

For the most part these differences are minor. The major characteristics of OTH targets and noise are reasonably well reproduced using the data model. Thus we feel justified in using this model for comparative evaluation of detection and tracking systems. The first use of this model was directed toward determining the detection sensitivity of the ERS display.

2. Display Sensitivity

The data model is able to create displays of realistic targets with specified average SNR and fluctuation levels, and is thus ideally suited for testing display sensitivity. For an initial test, a display of range (nested Doppler) vs time containing targets of 0 to 20 dB SNR was generated. Figures 12(a), 13(a), and 14(a) reproduce the displays, while Figures 12(b), 13(b), and 14(b) indicate track positions, SNRs, and fluctuation rates.

One useful measure of display sensitivity can be defined as the SNR required to obtain a 50% detection rate. From analysis of these data, it appears that the display sensitivity lies between 6 and 9 dB.

The test described above served to determine the range of SNRs that have marginal detection rates. In the coming months, additional simulations will be generated to obtain a more precise estimate of display sensitivity. These simulations will also be used to evaluate the display of Doppler (nested range) vs time as well as the WARF animated display. Finally, the data model will be used to test the automatic detection and tracking algorithm proposed for the ERS. Besides determining the sensitivity of this algorithm, it is hoped that we can gain insight into appropriate methods of interaction between the manual and automatic detection/tracking process.

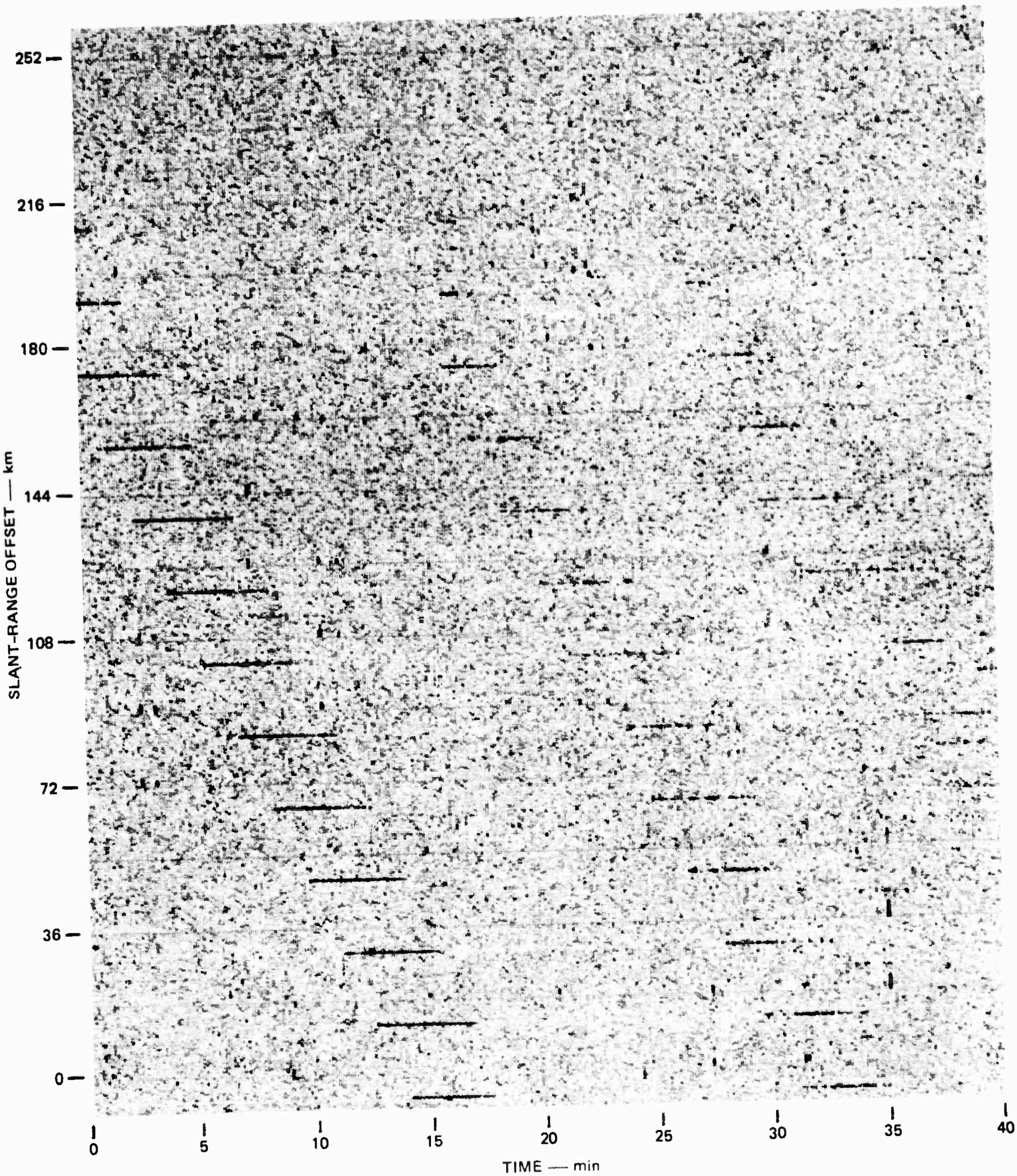

(a) RANGE (nested Doppler)-vs-TIME FORMAT — SIMULATED DATA WITH 8-s REFRESH

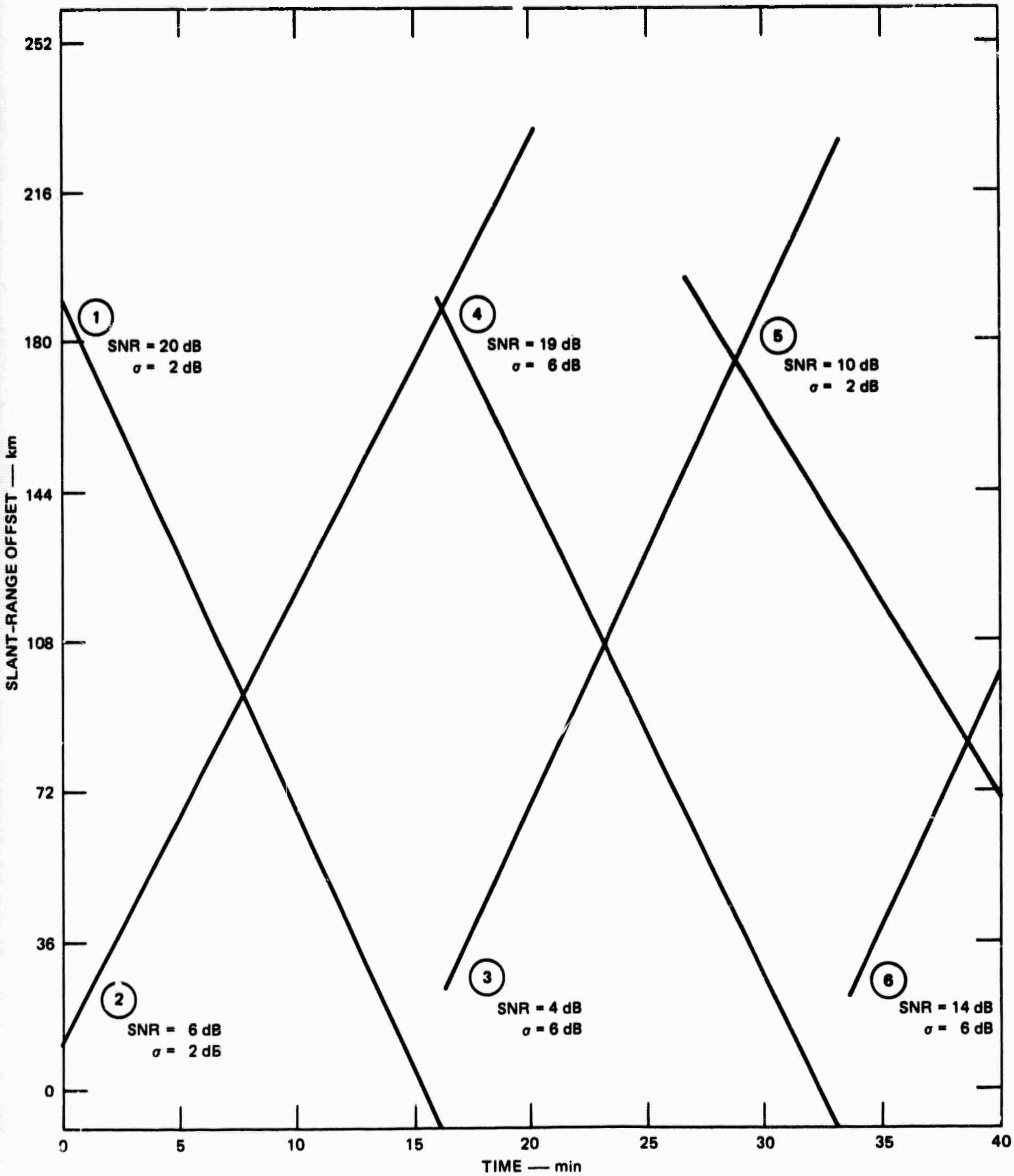

(b) TRAFFIC TEMPLATE FOR FIGURE 12(a)

FIGURE 12

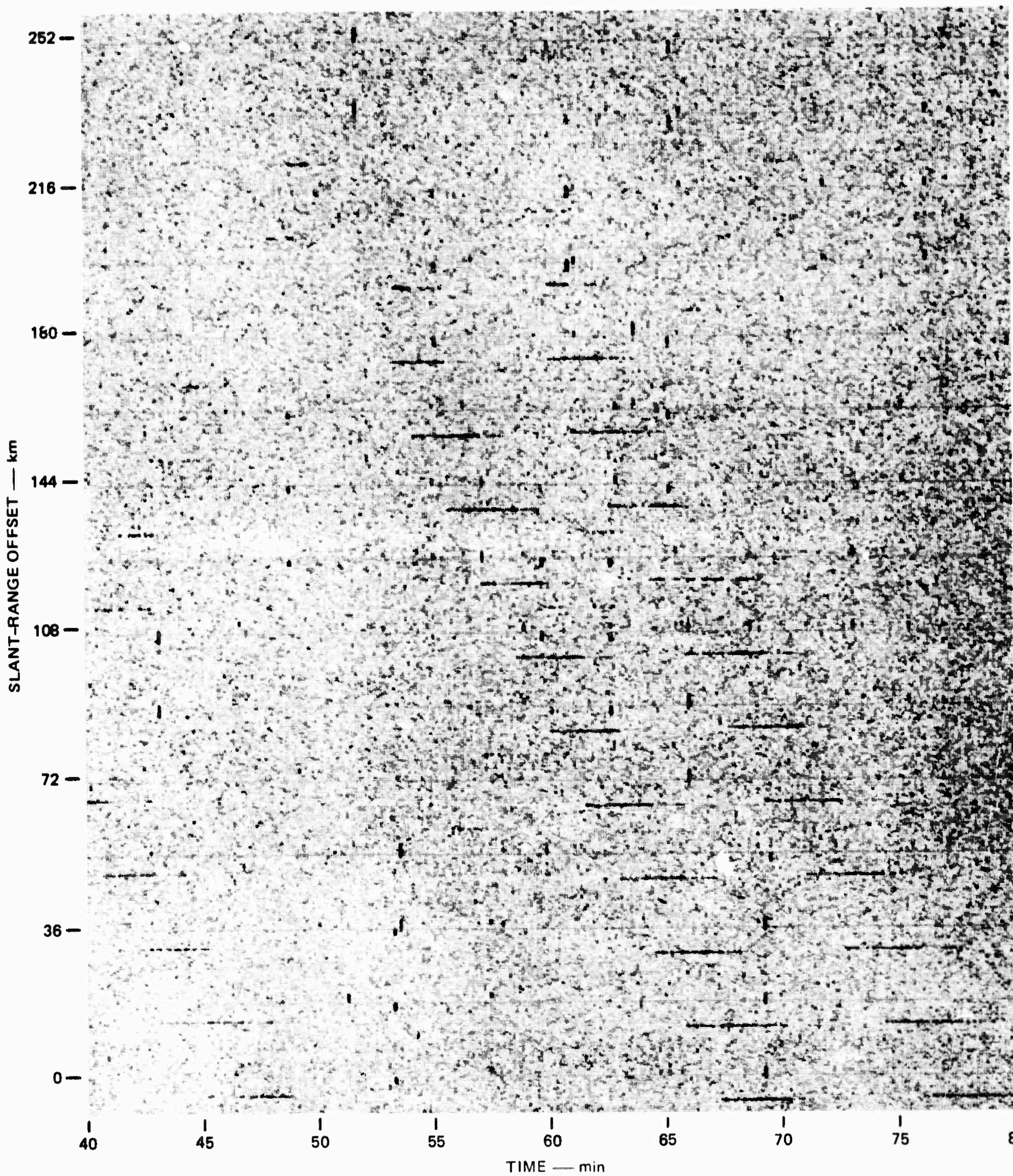

(a) RANGE (nested Doppler)-vs-TIME FORMAT — SIMULATED DATA WITH 8-s REFRESH

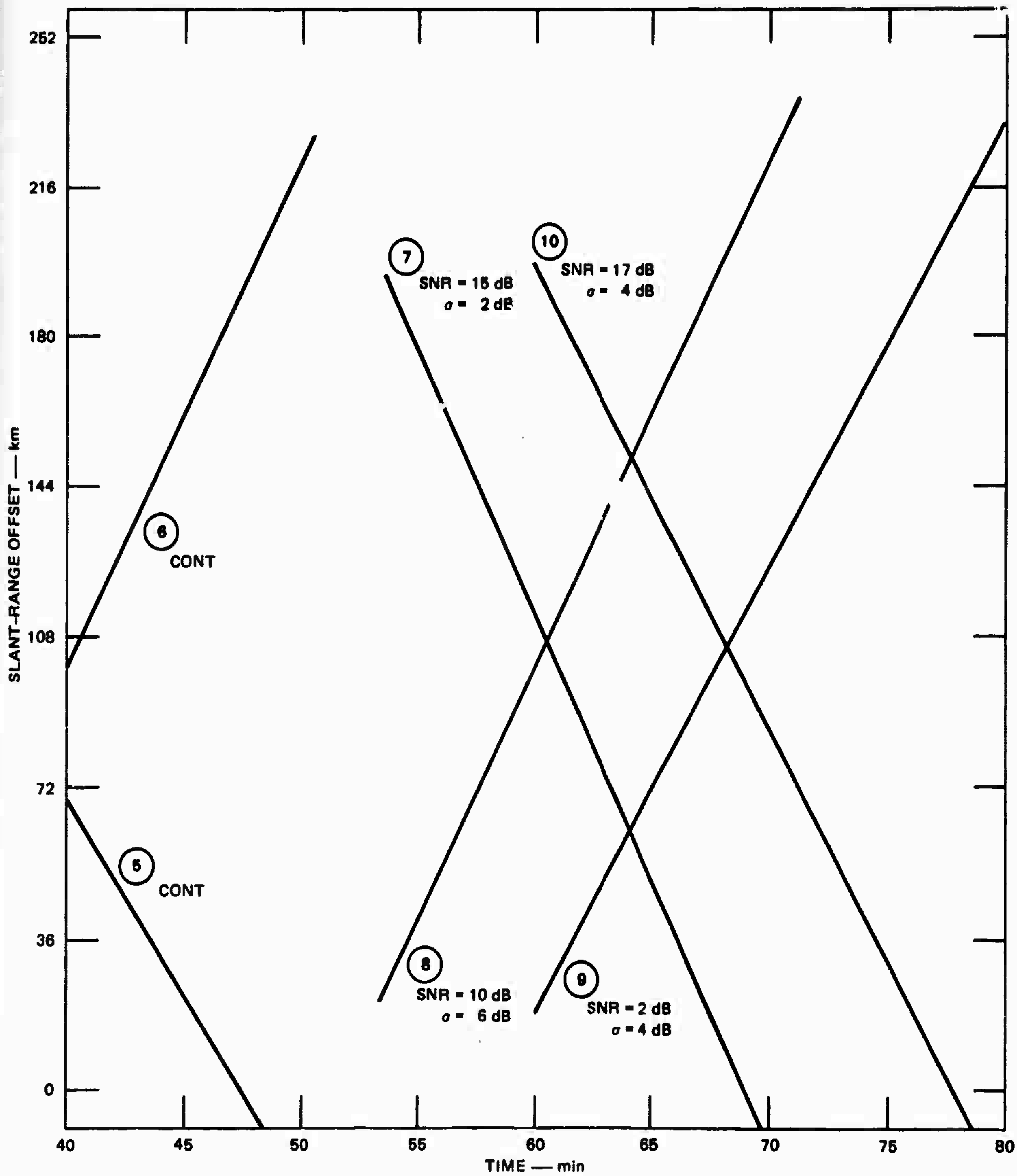

(b) TRAFFIC TEMPLATE FOR FIGURE 13(a)

FIGURE 13

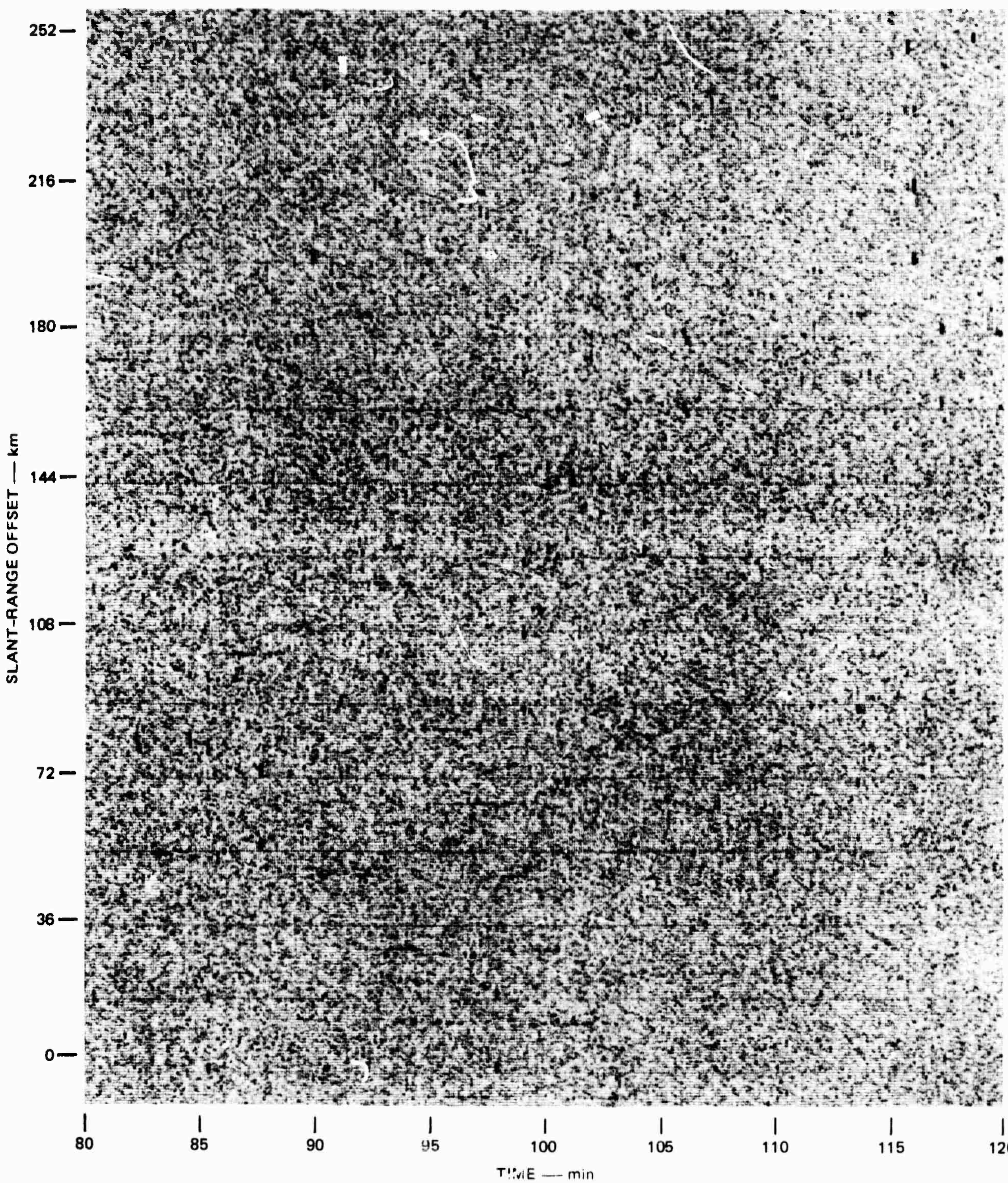

(a) RANGE (nested Doppler)-vs-TIME FORMAT — SIMULATED DATA WITH 8-s REFRESH

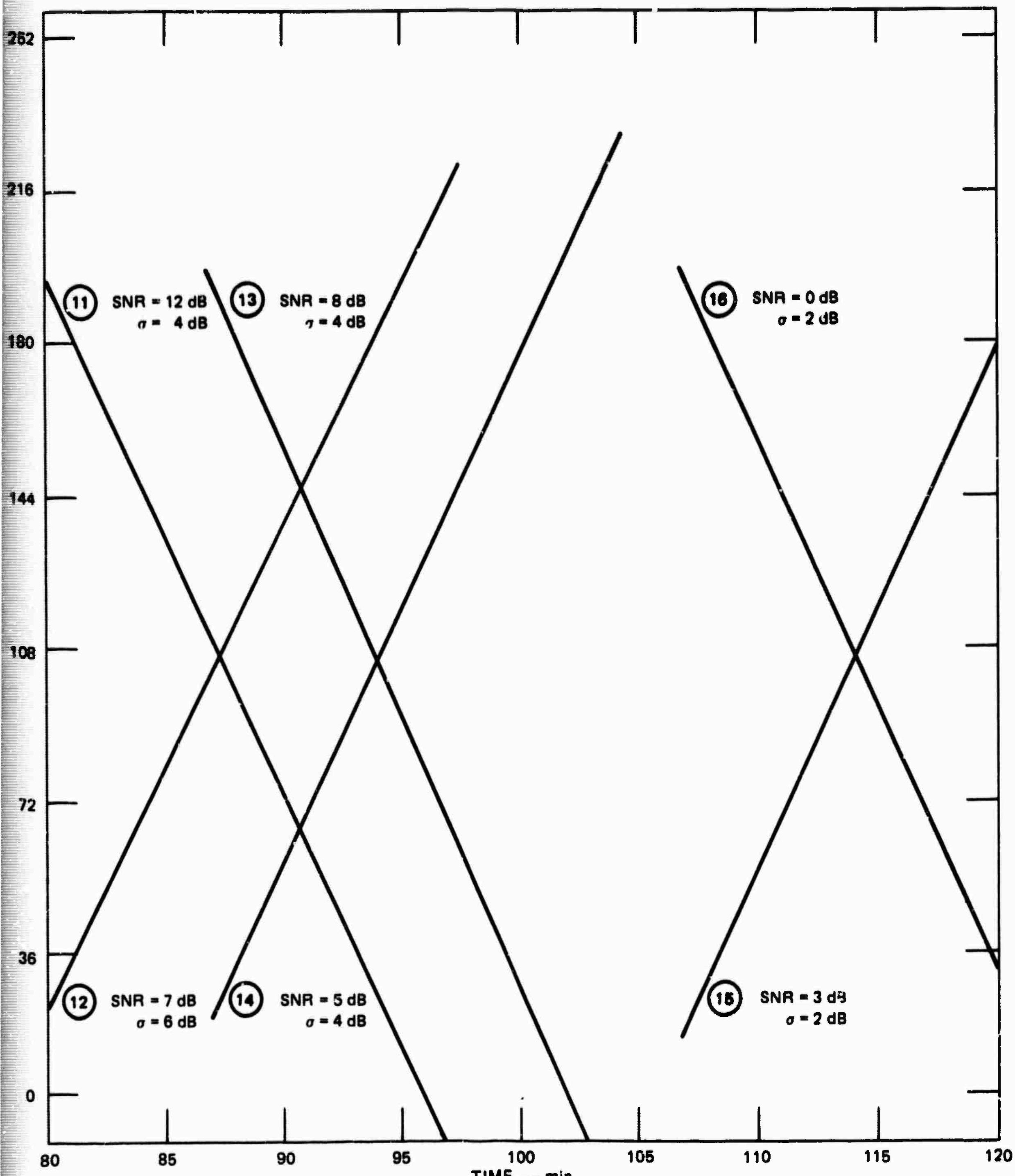

(b) TRAFFIC TEMPLATE FOR FIGURE 14(a)

FIGURE 14

D. Generalized Sidelobe Canceller

The University of Colorado (UC) under subcontract to SRI has developed a new adaptive noise-cancelling scheme referred to as a Generalized Sidelobe Canceller (GSC). This approach to adaptive signal processing may have application to OTH radars operating in the presence of auroral clutter. This brief description of the GSC processor will focus on its conceptual attributes; an in-depth analysis will be presented in a future UC report. In the meantime, while the GSC structure is under development at Colorado, a version of this processor has been implemented in software at SRI for off-line processing of WARF data and for preliminary performance evaluation.

Figure 15 is a simplified diagram of the GSC processor. A multidimensional input signal $\underline{X}$ as a function of time κ in the present application represents the signals received at an array of spaced antennas. This array or vector of input si ls is fed through two signal paths simultaneously, referred to as the upper and lower paths of Figure 15. The function of the lower path is first to apply a spatial preprocessing filter $\underline{\underline{W}}_s$ to the data in order to remove the desired signal from the data. The residue at the output is termed noise or unwanted energy. These data are fed through an adaptive feedback loop ($\underline{\underline{W}}_A$), which in general involves both spatial and time-domain filtering, to generate a beamformed output $Y_A(k)$.

The processing functions of the upper loop are a beamforming opera- $\underline{W}_C$ followed by a feedback tapped-delay-line $\underline{W}_B$. The output of the upper path $Y_c'(k)$ is subtracted from the lower path output $Y_A(k)$ to generate the final GSC output signal, $Y_o(k)$. Note that $Y_o(k)$ serves as the feedback error signal to update the adaptive weights in both the upper and lower paths. The weight-updating algorithm for the lower path is the least-mean-squares (LMS) algorithm,[3] while weight updating for the upper path may take on several forms.

The lower path serves as an error beam (or perturbation signal) so that if unwanted signals are present, the process of subtraction $Y_A(k)$ from $Y_c'(k)$ will remove such signals from the final output. If no such

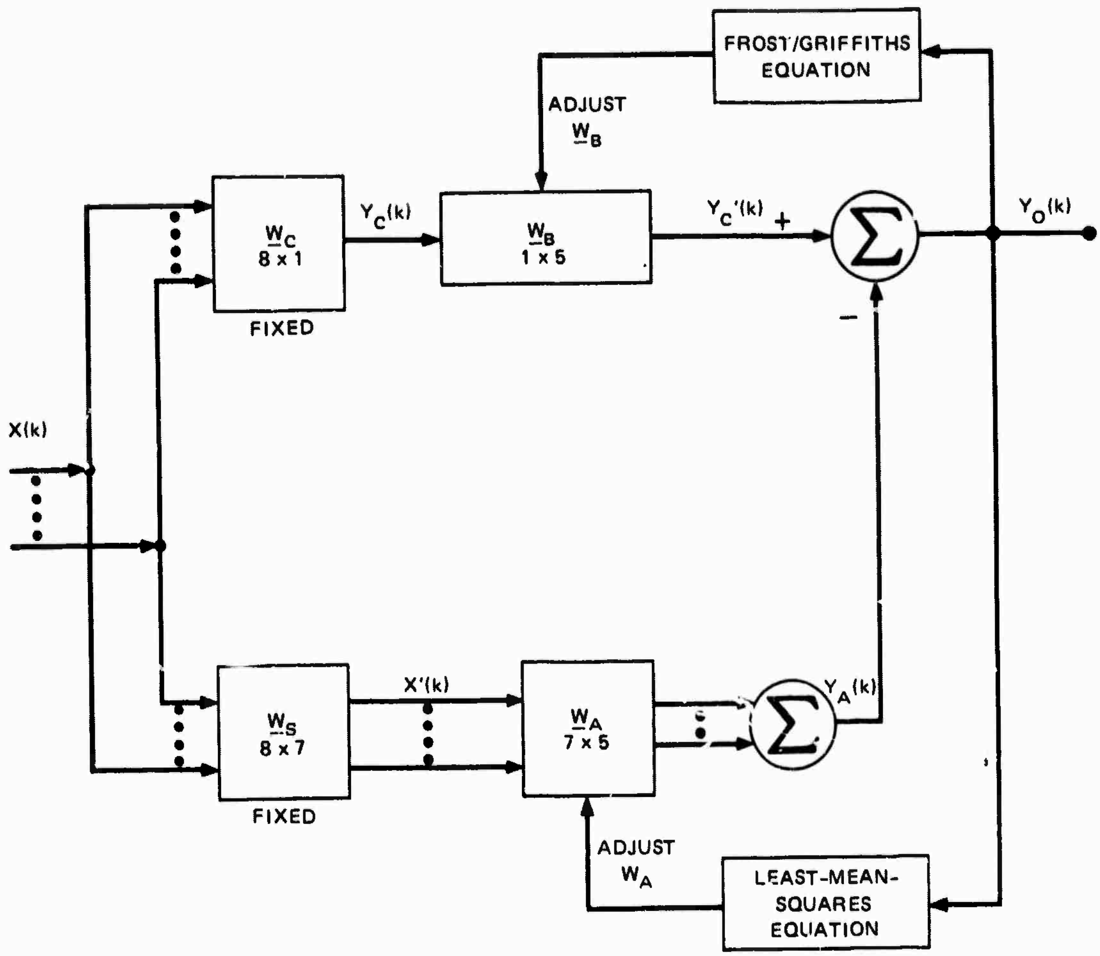

FIGURE 15 GENERALIZED SIDELOBE CANCELLER

signals are present, the error beam automatically shuts down and the upper path continues to process the input signals in a manner similar to that of a conventional beamformer.

One of the most promising aspects of this processor structure is that it permits the realization of a fairly general class of adaptive beamforming algorithms with a single unifying analytical approach. This feature greatly enhances the ability to compare the effect of different approaches to adaptive beamforming, something that has not been readily possible in previous work. For example, it is now quite easy to make this beamforming structure realize the Frost algorithm or the Griffiths algorithm, two previously studied approaches to adaptive beamforming.

Details of these versions of the GSC will be presented in a technical report devoted to this subject.

One current area of interest at UC is the form that the spatial preprocessing matrix $\underline{\underline{W}}_s$ should take in order to most effectively remove the wanted signal from the error beam One of the simplest versions is to use this filter to combine the array outputs in pairwise monopulse fashion--that is, element 1 is subtracted from element 2, element 2 is subtracted from element 3, and so on. A plane-wave signal in phase across all array elements will be removed by this process, leaving the so-called unwanted signals or noise. At UC Griffiths has shown how multielement generalizations of this monopulse-like spatial preprocessor may be realized using Walsh functions.

The GSC has been implemented in minicomputer software at SRI for off-line processing of WARF data. This implementation is quite general and flexible, to facilitate comparison of different realizations of the various component parts of the GSC. The present configuration has the following options:

• $\underline{W}_c$ weights	Uniform or Dolph
• $\underline{W}_B$ and $\underline{\underline{W}}_A$	Structured to realize either Frost or Griffiths algorithms with 8 elements and 5 taps
• $\underline{\underline{W}}_s$	Pairwise monopulse, Walsh functions, or manually selected at program initiation
• Elemental power equalization	Signals at output of $\underline{\underline{W}}_s$ have integrate-and-dump normalization with operator-selectable exponential time constant (usually 100 samples)
• Range-Doppler analysis	$Y_o(k)$ is applied to a 2-s (4096-sample) range-Doppler
• Output display	Either range-Doppler map or Doppler power spectrum.

Debugging of this processor was achieved in May through the use of taped artificial data designed to simulate both desired and unwanted signals arriving at an 8-element array with 320-m spacing. Based on these successful tests, the GSC was used in a preliminary test of beamformer performance against azimuthally spread ground clutter; the results of this test are described in Section II-E.

Two tests of the GSC processor were carried out with the aid of simulated signals. In the first test, two sinusoidal signals were injected into the eight input channels, one signal in-phase across the eight channels (in-beam), and the other signal with a linear phase shift to make the signal appear 1.5° away from the beam pointing direction. Gaussian noise was added so that the SNR of the in-beam signal was 30 dB when measured after beamforming and a 4096-sample coherent integration ($\simeq$2 s). The out-of-beam signal would have had a 50-dB SNR if it were in the beam. The desired (in-beam) signal was at a frequency of 420 Hz, and the unwanted signal at 400 Hz. In the second test all conditions were identical except that both signals were given element-to-element amplitude and phase randomization (10% and 15° respectively). This randomization was different for each of the two signals and it was fixed in time throughout the 4096 samples. Its purpose was to simulate typical departures from equal amplitude and linear phase front that are seen in real signals.

These signals were applied to the GSC using both the Griffiths and Frost beamforming algorithms with variable gain (α) in the weight-recursion loops. Conventional weights $\underline{W}_c$ were 25-dB Dolph coefficients; the W_s preprocessing filter was the pairwise-monopulse matrix--i.e.,

$$\underline{\underline{W}}_s = \begin{array}{c} \overleftrightarrow{\qquad 8 \qquad} \\ \begin{bmatrix} 1 & -1 & 0 & 0 & 0 & 0 & 0 & 0 \\ 0 & 1 & -1 & 0 & 0 & 0 & 0 & 0 \\ 0 & 0 & 1 & -1 & 0 & 0 & 0 & 0 \\ 0 & 0 & 0 & 1 & -1 & 0 & 0 & 0 \\ 0 & 0 & 0 & 0 & 1 & -1 & 0 & 0 \\ 0 & 0 & 0 & 0 & 0 & 1 & -1 & 0 \\ 0 & 0 & 0 & 0 & 0 & 0 & 1 & -1 \end{bmatrix} \end{array} \updownarrow 7 \quad .$$

The time constant of the individual channel gain normalization was 100 samples.

Figure 16 presents the Frost algorithm results. SNR is plotted for loop gain α for both desired and unwanted signals and for both ideal and randomized amplitudes and phases. Desired signal SNR remains near 30 dB at small values of α but begins to decrease sharply for $\alpha > 0.1$. This reduction in SNR is expected and is caused by adaptation noise. Cancellation of the unwanted signal is complete at $\alpha \simeq 0.001$ for ideal signals and $\alpha \simeq 0.005$ for the randomized signal. These results indicate that the correct gain has a fairly wide range of acceptable values centered around 0.01.

Corresponding plots for processing via the Griffiths algorithm are given in Figure 17. The overall trends are similar to those for Frost processing except that a slightly larger value of α is required for the Griffiths processing to achieve the same amount of rejection. Once again, higher α is required to remove the unwanted signal for the randomized signal case. One notable feature of Griffiths beamforming is that SNRs for both signals appear larger than those measured for the conventional beamformer. This behavior is caused by the tapped-delay-line filtering, which is an integral part of the Griffiths algorithm and which produces filtering (i.e., noise cancellation) in the frequency domain. The noise-measurement algorithm used for these data computes an rms value over the whole frequency band, and the computed noise values may be decreased since some noise is cancelled during adaptation. The bias in noise values could be removed by measuring noise at the mid-frequencies of the receiver passband (~420 Hz), but since both wanted and unwanted signals are referenced to the same noise measurement it is of no consequence.

These results are in general accordance with the expected performance of the GSC for the simulated signals used in the test, and therefore it is concluded that the SRI implementation is functioning properly. Furthermore, these results establish the desired amount of feedback in the weight-recursion algorithms.

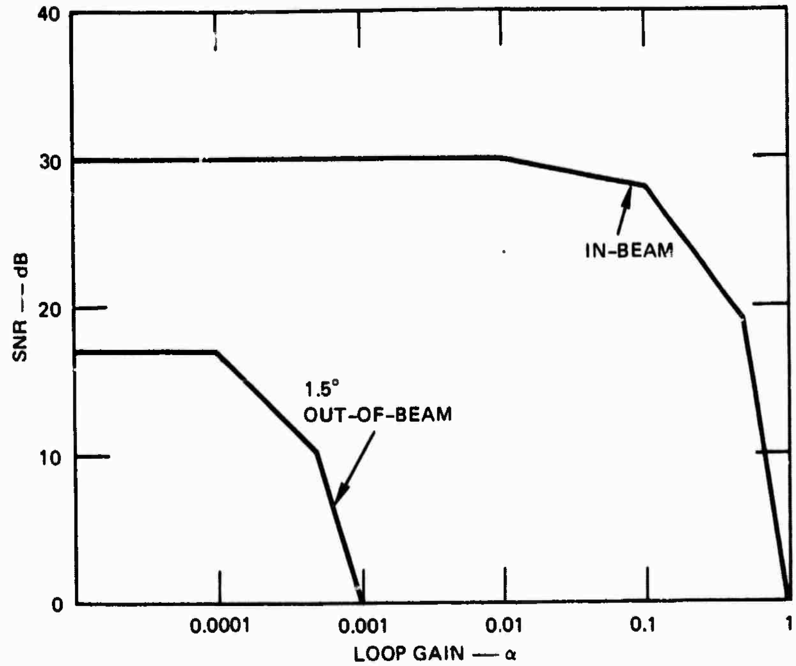

(a) IDEAL SIGNALS (IN-BEAM SNR = 30 dB; OUT-OF-BEAM SNR = 17 dB)

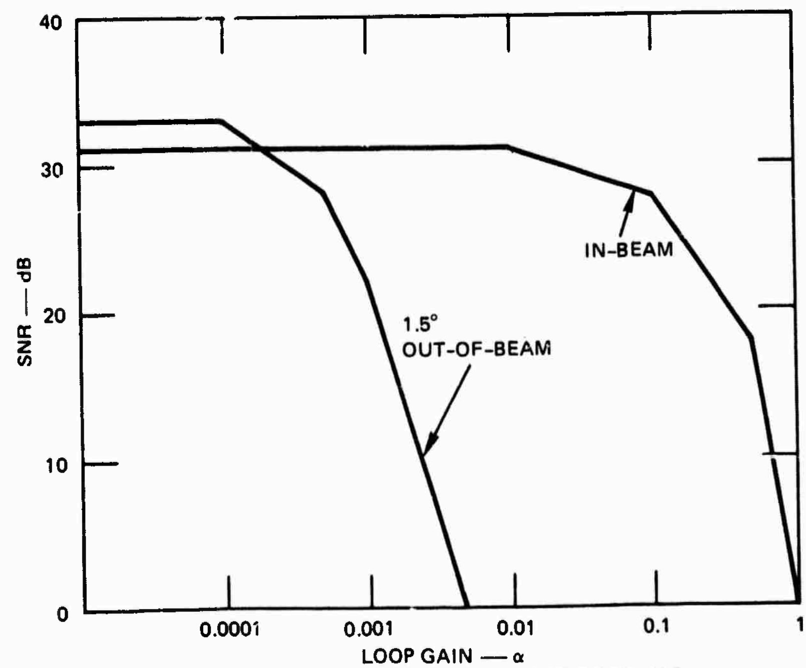

(b) AMPLITUDE AND PHASE RANDOMIZED SIGNALS (IN-BEAM SNR = 31 dB; OUT-OF-BEAM SNR = 33 dB)

FIGURE 16 PERFORMANCE OF GSC PROCESSOR (Frost Algorithm) AGAINST SIMULATED SIGNALS

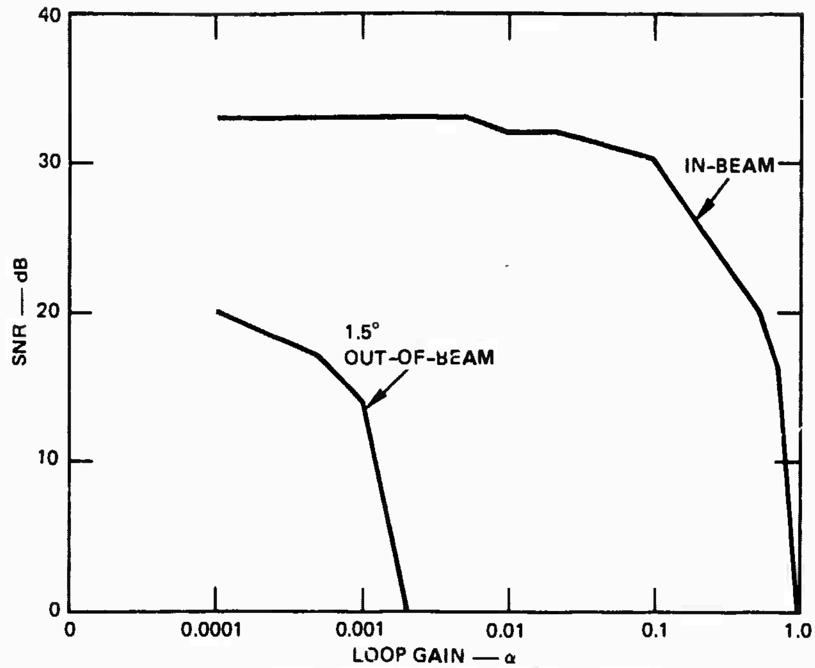

(a) IDEAL SIGNALS (IN-BEAM SNR = 30 dB; OUT-OF-BEAM SNR = 17 dB)

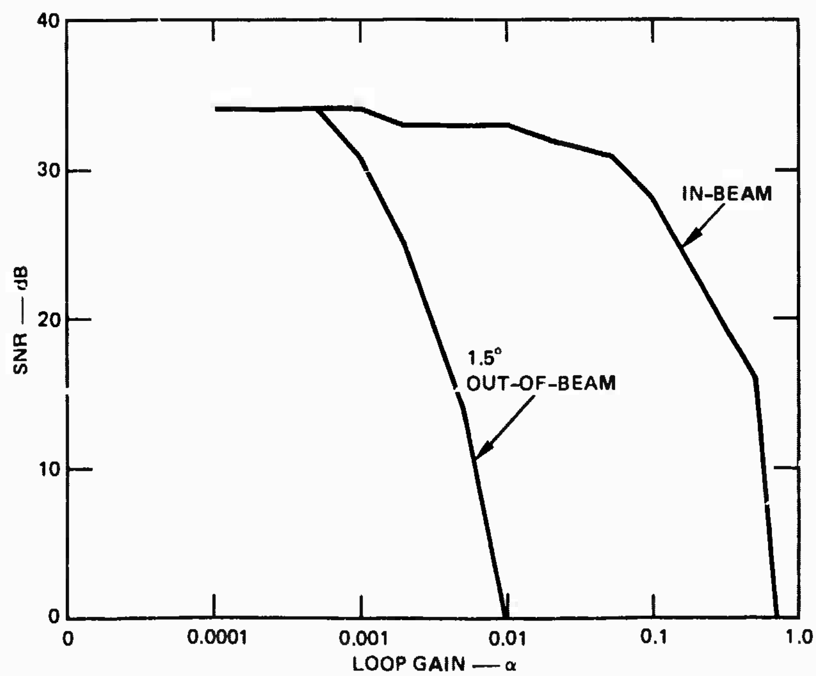

(b) AMPLITUDE AND PHASE RANDOMIZED SIGNALS (IN-BEAM SNR = 31 dB; OUT-OF-BEAM SNR = 33 dB)

FIGURE 17 PERFORMANCE OF GSC PROCESSOR (Griffiths Algorithm) AGAINST SIMULATED SIGNALS

E. Spread Clutter Effects on Adaptive Beamformers

One of the primary reasons for applying adaptive beamforming techniques to HF radar is to exploit their potential for rejecting spread-azimuth and spread-Doppler clutter such as that produced by scattering from auroral irregularities. While it is relatively easy to implement point-source interferers for performance testing of a candidate beamforming technique, it is not convenient to generate a realistic spread-azimuth interference source. Computer simulation studies have been undertaken at SRI to analyze the degree to which various methods of adaptive beamforming could be expected to work against such unwanted energy. Yet the simulation results are not fully convincing in their ability to account for all the aspects of the actual HF environment and the achievable performance of HF equipment. Experimental results are highly desirable.

Consideration has been given at SRI to determining how the WARF adaptive beamforming capabilities could be used to test ways to reject spread-azimuth interference. Possible ways to address this problem experimentally include the following:

(1) Use a separate transmitter--The WARF could be configured to look at desired targets such as a repeater while a remote transmitter operating on the same frequency is located to make energy arrive through the sidelobes of the receive beam. If this out-of-beam signal propagates via a 2-hop path, then some azimuthal and Doppler spreading of the unwanted signal will result. Depending primarily on the transmit beamwidth and the terrain roughness at the midpath point, the azimuthal spreading of the remote transmitter signal could amount to several degrees.[4]

(2) Mis-steer the WARF transmit beam--The log periodic array at Lost Hills has a 6° azimuthal beamwidth (at 15 MHz) with average sidelobes 20 to 25 dB down. By the simple expedient of shifting the transmit steer direction away from the direction to the desired signal, a clutter distribution with significant out-of-beam components can be produced at the Los Banos receive site. The out-of-beam clutter has about 6° azimuthal width and a Doppler spectrum like that of normal land or sea backscatter.

(3) Gather data in the presence of spread ionization--Even at the moderate latitude of WARF (55° magnetic), ionospheric phenomena similar to those observed in the auroral regions are present. Scatter from spread-F ionization is observed frequently; and reflections from these irregularities

produce spreading in Doppler and in azimuth. Data collection in the presence of such phenomena could emulate almost exactly the eventual operational environment of interest to the Air Force.

(4) Use the Boulder ionospheric heater--Ionospheric heaters generate field-aligned ionospheric irregularities very much like those found in auroral regions. A critical and unique aspect of these artifically induced irregularities (and therefore sources of clutter) is that they are controllable--i.e., they may be turned on and off at will. This property makes heater-induced spread clutter more desirable than naturally occurring spread clutter at least for purposes of evaluating beamforming techniques.

At the present time only the first alternative--a separate transmitter--has been rejected, principally because of the anticipated difficulties in frequency management for simultaneous one-hop and two-hop paths. Mis-steering of the transmit beam, while not fully realistic, is inexpensive and simple to test. Some WARF data collected with this configuration are described in Section II-F, below. The third and fourth options of collecting data in the presence of natural or artificial spread clutter may be tested in FY78.

F. Mis-Steered Transmitter Beam

Steering the transmit beam away from the desired target (the Los Lunas New Mexico repeater in this case) produces substantial ground clutter, which is received through sidelobe angles. This clutter has azimuthal extent at least as large as the transmit beamwidth (6°), and in the frequency domain consists of about 1-Hz-wide components spaced at the waveform repetition rate. This situation provides a preliminary test of beamformer capability to reject spread clutter.

The WARF was operated as in earlier adaptive beamforming experiments[5]--that is, essentially in an aircraft detection mode with the exception of the eight-channel coherent receiving system. In Phase 1 of the test the transmitted beam was pointed at the repeater as accurately as possible while several data files of the receiver outputs were recorded digitally. Sequential files were recorded as the conventional array pointing direction was stepped ±1/4° from the nominal azimuth to the New Mexico repeater; this maneuver is included to ensure that the repeater echo is closely aligned to the pointing direction in at least one of three sequential data files. Phase 2 of the test repeated the sequential stepping of the receive look direction while the transmit steer was misaligned by 12°. The sketch in Figure 18 illustrates the the time sequence of the test.

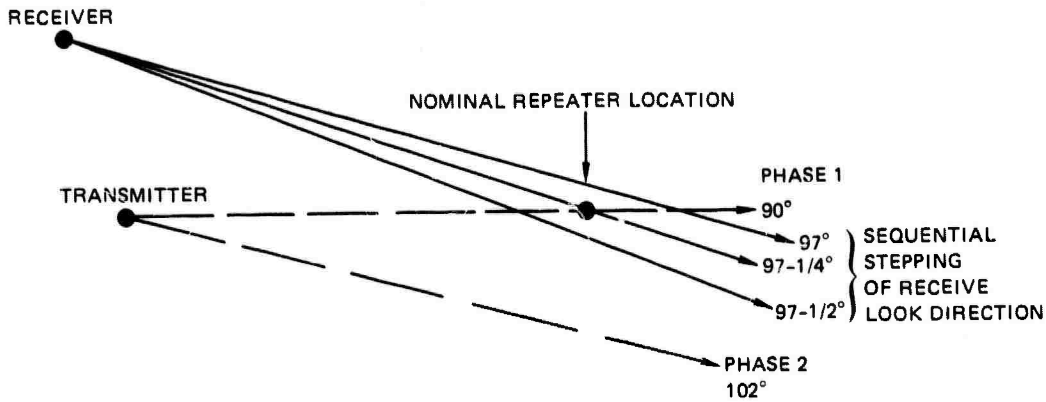

FIGURE 18 GEOMETRY OF TRANSMITTER MIS-STEERING TEST (not to scale). At 15 MHz, receive beamwidth is 0.5° and transmit beamwidth is 6°.

Over a period of 6 minutes, 72 two-second coherent-integration periods were acquired, 36 with the transmitter beam pointing as close to the repeater as possible and 36 with the beam misaligned by 12°. The repeater gain was increased by 30 dB during the misaligned portion of the test in order to maintain repeater SNR at a mean value of 25 dB over both portions of the test. Clutter-to-noise ratio (or subclutter visibility) decreased by more than 20 dB when the transmitter beam was missteered. Figure 19 presents typical samples of total power spectra for the two phases of the test; these spectra were obtained using conventional beamforming and a 2-s (or 128-sweep) coherent integration time.

A version of the Generalized Sidelobe Canceller (GSC) beamformer was applied to these data. A $\underline{\underline{W}}_s$ matrix consisting of pairwise monopulse weights (described in Section II-D) was used to cancel the desired signal in the error (perturbation) beam processing path. The Frost algorithm

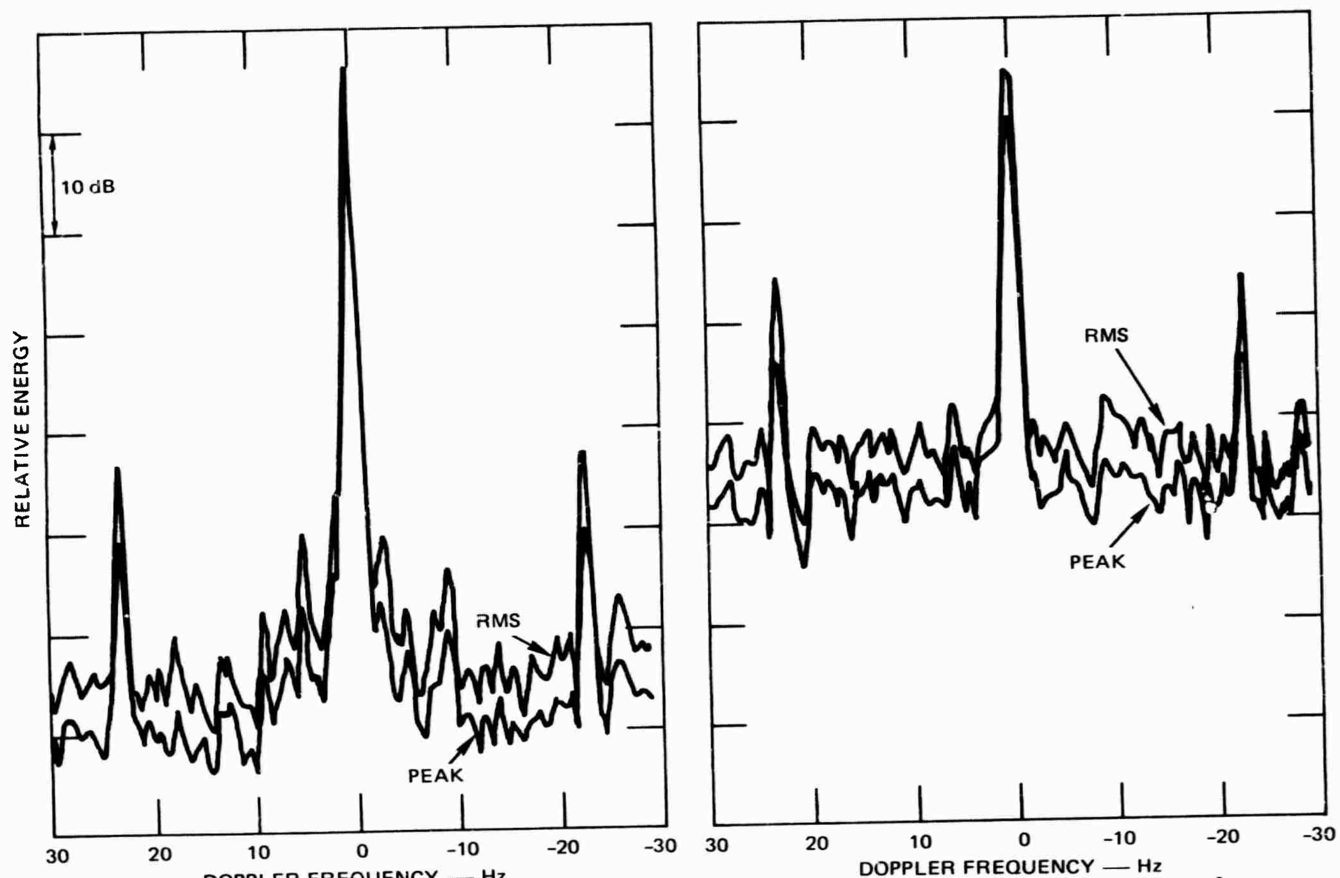

(a) TRANSMITTER BEAM ALIGNED WITH REPEATER

(b) TRANSMITTER BEAM MIS-STEERED BY 12°
(REPEATER GAIN INCREASED TO MAINTAIN SNR)

FIGURE 19 TYPICAL DOPPLER POWER SPECTRA OBSERVED DURING THE CLUTTER-CANCELLATION TEST OF THE GSC PROCESSOR using 35 weights (seven elements, five taps) with $\alpha = 0.1$ was applied to this error signal to provide the error beamformed output. This output was subtracted from the conventional beam and the result underwent range-Doppler analysis as in the conventional case.

Table 1 summarizes the data analysis for the two sets of data by presenting average values of SNR and signal-to-clutter ratio (SCR). In each case, signal is defined as the peak signal amplitude; clutter is defined as the maximum value (over Doppler) of the rms range average of clutter magnitude (rms over 216 km), and noise is defined as the rms of noise over regions of range and Doppler sufficiently removed from clutter and targets. These quantities are measured after range-Doppler analysis, and in order to refer them to the point of beamformer output we subtract 33 dB from SNR and 20 dB from SCR. Since processing gain affects both conventional and adapted channels equally, comparisons are made after range-Doppler analysis. These quantities are in fact measured from data plots such as those in Figure 19.

Table 1

DATA SUMMARY FOR MIS-STEERED TRANSMITTER BEAM TEST

	Transmit Steer 90°	Transmit Steer 102°
Conventional SCR (dB)	-32	-14
SCR Improvement (dB)	8	11
Conventional SNR (dB)	25	26
SNR Improvement (dB)	-3.9	0.3

In Table 1, improvement in SNR and SCR refers to increases in these quantities through adaptive beamforming over those achieved by conventional beamforming. On the average, the SCR improvement is 8 dB with beam alignment, increasing to 11 dB with beam misalignment. The SCR improvement with beam misalignment would in all likelihood be larger if the conventional SCR had been constant, since it is known that the potential for adaptive beamformer improvement is larger for small ratios of desired signal to unwanted signal at the input to the processor. Thus, if conventional SCR could have been maintained at -32 dB when the beam was mis-steered, then SCR improvement should have increased more than from 8 to 11 dB. The point here is that even with the presence of quasi-grating lobes the adaptive beamformer achieves cancellation of the spatially extended ground clutter.

A related quantity of interest is SNR, which is expected to remain constant if the noise is spatially isotropic. However, if the repeater signal is not precisely within the received beam, the beamformer may partially reject the signal, and, furthermore, with high gain (α) in the adaptive loop some adaptation noise may be added. SNR improvement with beam misalignment is virtually 0 dB as expected; however, with beam alignment it is -4 dB. Since the data conditions were identical for both data sets, it is conjectured that the larger value of clutter (relative to the signal) for the data with transmit beam alignment has produced more adaptation noise. This source of noise is reduced with smaller values of α; however, lower α may possibly reduce the achieved amount of SCR improvement.

This preliminary test of the GSC performance against spatially spread clutter is not conclusive, but it is encouraging. First, some portion of the clutter is either within the beam-pointing direction or within a quasi-grating-lobe pointing direction, and therefore an adaptive beamformer can only partially cancel the clutter. Thus, this test cannot be expected to measure the achievable amount of cancellation of out-of-beam spatially spread clutter. Second, the frequency spread of this type of clutter consists of discrete frequencies spaced at the waveform repetition rate with minor Doppler spreading (1 to 2 Hz) about these frequencies. Ultimately we would like to measure performance against clutter with larger Doppler frequency spreading. On the other hand, this result does show that appreciable cancellation of azimuthally spread clutter is achievable. Future experimentation will seek to determine expected performance levels in a more realistic experimental environment.

III CONSULTING ACTIVITIES

During the six months covered by this report SRI provided a variety of services requested by the SPO under the consulting portion of this contract. The following is a brief description of each of the major consulting tasks:

(1) Cost-Savings Effort--Because of growing costs, the Prototype Radar System (PRS) design was substantially modified to the current Experimental Radar System (ERS) design. SRI International supported this effort by participating in meetings at the SPO, providing timely data to the SPO for high-level briefings, and presenting technical opinions in response to requests from the Office of the Assistant Secretary of the Air Force for Research and Development.

(2) Long-Path Soundings--At the request of ESD, SRI provided approximately 200 hours of sounding transmissions from the WARF Lost Hills transmit facility. These soundings, requested by Dr. Elkins of RADC, were received on RADC equipment at Ava, New York and later overseas.

(3) Transponder Design--It had been proposed that SRI supply the Air Force with transponders for use in the ERS coverage. Preliminary design and cost estimates were developed during this reporting period.

(4) Environmental Assessment System--SRI developed a technical concept for augmenting the ERS with an independently operated environmental assessment system (EAS). This would be a minicomputer-based system designed to improve ionospheric propagation management capabilities at the ERS.

Appendix A

ARCHITECTURE FOR A HARDWARE BEAMFORMER

Appendix A

ARCHITECTURE FOR A HARDWARE BEAMFORMER

As a part of the ongoing analysis of adaptive beamformers at SRI, a study has been initiated to define how an on-line beamformer might eventually be best implemented. During this reporting period the structure of the GSC was used as a candidate for possible on-line implementation in order to obtain a measure of cost, speed, and performance of such a device when integrated into the operation of an OTH radar.

The particular structure of the generalized sidelobe canceller has led to the suggested design of a multipler-oriented processor shown in Figure A-1. This design takes advantage of the fact that many of the algorithm operations are of the form of a weight term times a data or output term. This simplifies the splitting of memory into two parts, one a data memory and one a weight memory, which decreases the access time for the multiplier and multiplicand. Also some of the equations involve accumulating the products of data and weights for up to 35 operations, with the results stored in either memory. This fact led to the design of the product summation unit as an adder-subtractor-accumulator with access to either memory.

Some of the algorithms involve summing data in memory. This could be accomplished by multiplying by 1 if integer arithmetic is assumed, or by the largest positive fraction if fractional arithmetic is assumed, or by -1 and subtracting the result if integer arithmetic is assumed. An easier method is to allow the memories to have direct access to the accumulator through a bus and selection arrangement. This method permits easier and quicker summation of nonmultiplied terms.

In order to prevent any loss of accuracy, the accumulator must be designed to handle the summation of up to 35 products, each product having 23-bit resolution, resulting in 29 bits of storage for the accumulator. The output to memory can contain only 12 bits, since integer

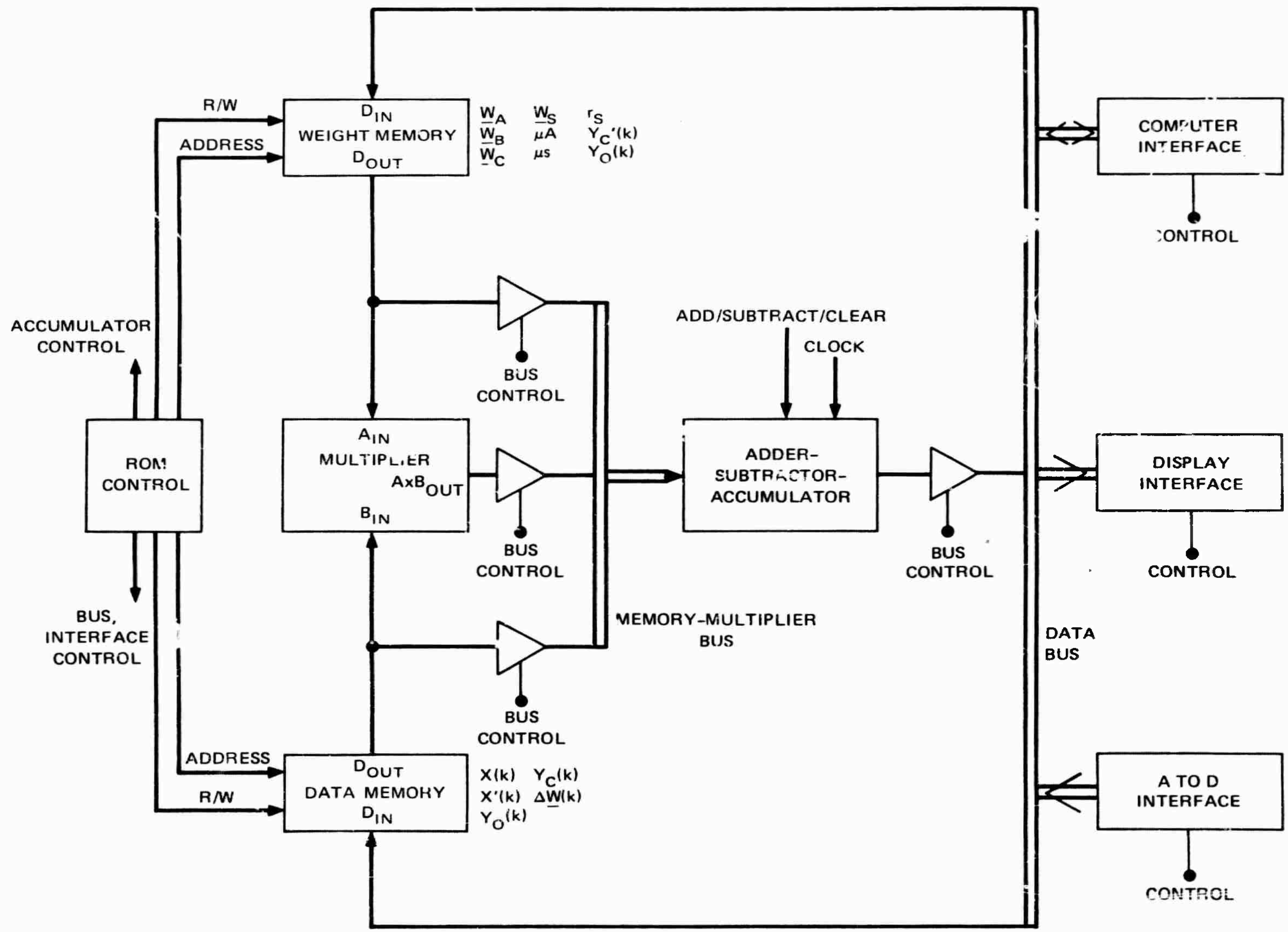

FIGURE A-1 ARCHITECTURE FOR AN OPERATIONAL GENERALIZED SIDELOBE CANCELLER arithmetic is assumed, and must therefore be truncated or rounded. This illustrates the usefulness and necessity of the floating-point approach in minimizing the errors due to truncation, rounding, or an arbitrary selection of bits.

The control of the multiplier, accumulator, and data buses would be done with Read Only Memory (ROM). The ROM, addressed by a counter, would determine the addresses for each memory and would control the bus access of each memory or multiplier output. Addresses for data storage as well as read-write controls are also generated. Control of the accumulator operation by the ROM provides clear accumulator, accumulator-to-output-bus, sum-input, and subtract-input signals.

The ROM would also control the data output bus and peripherals such as the analog-to-digital converter (ADC) interface, display interface, and interface to the main processor computer. The ADC is a stand-alone unit controlled by its own microprocessor or microprogrammed controller. This peripheral would acquire a set of eight data samples, perform any necessary digital filtering, and signal the GSC controller that a set of data samples is ready. The computer interface communicates to the system computer and transfers the adapted beamformed data to the main computer for further analysis (such as range-Doppler processing) and output to a display. There would also be a transfer of control information or data from the main computer to the GSC. This would enable the main computer to alter or adjust the adaptive algorithms or use the GSC as an external data processing unit.

By examining the structure of the GSC and the equations required, it can be seen that each data set (eight inputs from the ADC) requires 195 multiplications and 196 summations or subtractions. Since this arithmetic must be executed in less than 500 μs, a fast controller is needed to address memory, control the accumulator and bus, and control the peripherals. The ROM can do this because of its rapid access times. The complexity of the operations and the desire to modify the algorithm operation in real time suggest that a microprocessor-based controller should be used. However, most MOS microprocessors are too slow for this application, having instruction times of 1 μs or more. In contrast, a bipolar microprocessor slice or microprogram sequencer could be used to control the GSC. This alternative would permit adjustment of parameters to optimize GSC performance according to operational needs.

Appendix B

GENERALIZED SIDELOBE-CANCELLER-SYSTEM MULTIPLIERS

Appendix B

GENERALIZED SIDELOBE-CANCELLER-SYSTEM MULTIPLIERS

The multiplier used in the adaptive processor must be able to form 23-bit products from 12-bit two's-complement input numbers. The number of multiplications required in each data update period (500 μs) is such that multiplier speed must be 2 μs or less.

Several multiplying schemes and implementations were studied* and compared on the basis of speed, power consumption, total size of multiplier, and total costs. For comparison, methods that do not use two's-complement arithmetic or that lack sufficient precision are included. Table B-1 lists the costs of space requirements (board layout costs, physical size of integrated circuits), components, power, and total size for several multiplying implementations, while Table B-2 lists the performance of these implementations.

Studies are continuing to determine the necessary accuracies needed in the GSC and to determine the usefulness of a floating-point system.

---

*"A Survey of Digital Multiplying Techniques," by Philip C. Evans. Unpublished internal report for A. M. Peterson and T. W. Washburn (June 1977).

Table B-1

CIRCUIT COSTS
(Dollars)

Design	Requirements Space	Integrated Circuit	Power	Total
Shaw's Serial-Parallel (S-P)	$23	$ 53	$11	$ 87
Robertson's S-P	24	38	9	71
Booth's 25LS14	19	80	15	114
AMD 2505	36	270	41	347
TI 74LS274	33	75*	15	123*
TI 74LS261	41	106*	23	170*
MM 67558 (4 units)	22	418*	22	462*
MM 67558 (1 unit)	24	137*	12	173*
TRW MPY 12AJ	4	165	18	187
Squaring circuit	28	113*	9	150*
Approximation†	15	24	7	46

*Estimates.

†Insufficient precision.

Table B-2

MULTIPLIER PERFORMANCE

Design	Multiplication Speed (μs)	Power (W)	Speed-Power (W-μs)	Speed-Power-Cost ($-W-μs)
Shaw's S-P	1.430	2.14	3.06	266
Robertson's S-P	0.960	1.68	1.61	114
Booth's 25LS14	1.000	2.92	2.92	333
AMD 2505	0.205	8.10	1.66	576
TI 74LS274	0.130	2.93	0.38	47
TI 74LS261	0.130	4.49	0.58	99
MM 67558 (4 units)	0.140	4.48	0.67	310
MM 67558 (1 unit)	0.770	2.32	1.79	310
TRW MPY 12AJ	0.193	3.50	0.68	127
Squaring circuit	0.225	1.86	0.42	63
Approximation	0.200	1.30	0.26	12

REFERENCES

1. W. B. Zavoli, E. A. Elpel, T. W. Washburn, and L. E. Sweeney, Jr., "A Technique for Producing Wide-Sweep Sensitivity Soundings with Applications to OTH-B Radar Propagation Management," Technical Report 32, Contract N00014-70-C-0413, SRI Project 8727, Stanford Research Institute, Menlo Park, California (November 1975).

2. W. B. Zavoli and D. E. Westover, "A Model for OTH-Radar Data," Technical Report 35, Contract N00014-75-C-0930, SRI Project 4062, Stanford Research Institute, Menlo Park, California (August 1976).

3. B. Widrow, P. E. Mantey, L. J. Griffiths, and B. B. Goode, "Adaptive Antenna Systems," Proc. IEEE, Vol. 55, pp. 2143-2159 (December 1976).

4. L. E. Sweeney, Jr., "Spatial Properties of Ionospheric Radio Propagation as Determined with Half-Degree Azimuthal Resolution," Technical Report 155, Contract Nonr-225(64) (NR 088-019) and ARPA Order 196, Stanford University, Stanford, California (June 1970).

5. T. W. Washburn, L. E. Sweeney, Jr., L. J. Griffiths, and D. E. Westover, "Adaptive Beamforming Techniques for HF Backscatter Radar," Technical Report 33, Contract N00014-70-C-0413 (NR 088-047), SRI Project 8727, Stanford Research Institute, Menlo Park, California (January 1976).

DISTRIBUTION LIST

Organization	Number of Copies
DEPARTMENT OF DEFENSE	
Office of the Deputy Under Secretary (Communications, Command, Control and Intelligence) Pentagon, Room 3E282 Washington, D.C. 20301	1
Office of the Deputy Under Secretary Research and Advanced Technology DDR&E Pentagon, Room 3E114 Washington, D.C. 20301	1
Office of the Director Defensive Systems, DDR&E ATTN: Mr. Robert C. Yost Pentagon, Room 3D136 Washington, D.C. 20301	1
Director Defense Advanced Research Projects Agency ATTN: STO, Mr. Eugene H. Kopf 1400 Wilson Boulevard Arlington, Virginia 22209	1
Director Defense Intelligence Agency	
ATTN: DC7	1
DT2B	1
Pentagon Washington, D.C. 20301	
Director National Security Agency	
ATTN: R5, Mr. J. G. Hengen/ Dr. John Pinkston	1
W23, Capt. R. Parenti	1
W32, Mr. C. H. Wilts/ Dr. Lee Edwards	1
Fort Geo. G. Meade, Maryland 20755	
Commandant Defense Intelligence School Washington, D.C. 20374	1
Defense Documentation Center Cameron Station Alexandria, Virginia 22314	2
Director Weapons Systems Evaluation Group 400 Army-Navy Drive Arlington, Virginia 22202	1

Organization	Number of Copies
DEPARTMENT OF THE NAVY	
Office of Naval Research	
ATTN: Code 427, Dr. Henry Mullaney	1
Code 461(FP), Mr. J. J. Kane	1
800 N. Quincy Street Arlington, Virginia 22217	
Office of Naval Research Branch Office ATTN: Mr. Stan Curley 495 Summer Street Boston, Massachusetts 02210	1
Office of the Assistant Secretary of the Navy (R&D) ATTN: Dr. Thomas P. Quinn Pentagon, Room 4E741 Washington, D.C. 20350	1
Office of the Chief of Naval Operations	
ATTN: OP-098D, Pentagon, Room 5D760	1
OP-942, Pentagon, Room 5E569	1
OP-955D/Capt. H. A. Hoover, USN Pentagon, Room 5D626	1
OP-955E/Cdr. V. S. Mazzola, USN Pentagon, Room 5D625	1
Washington, D.C. 20350	
Commander-in-Chief U.S. Atlantic Fleet Norfolk, Virginia 23511	1
Commander-in-Chief U.S. Pacific Fleet ATTN: Code 302 Makalapa FPO San Francisco, California 96610	1
Commander, Third Fleet	
ATTN: Code N22	1
Code N7644, Mr. F. Forsyth	1
Code OIT	1
Ford Island FPO San Francisco, California 96610	
Chief of Naval Material ATTN: NMAT 0311, Cdr. J. W. Hugo, USN 2211 Jefferson Davis Highway Arlington, Virginia 20360	1
Commander Naval Ocean Systems Center	
ATTN: Code 0104, Dr. Paul Moose	1
Code 1201, Mr. W. L. Hastings	1
Code 7141, Mr. H. J. Wirth	1
Code 721, Dr. Peder M. Hanson	1
San Diego, California 92152	

DISTRIBUTION LIST (Continued)

Organization	Number of Copies
Commander Naval Electronic Systems Command ATTN: 03/03A	1
03/034A	1
320A	1
52011A, Mr. G. N. Skillicorn	1
52023B, Mr. R. D. Blackburn	1
National Center No. 1 2511 Jefferson Davis Highway Arlington, Virginia 20360	
Commander Naval Missile Center ATTN: Code N03022	1
Point Mugu, California 93041	
Commander Naval Ocean Research and Development Activity ATTN: Code 600, Dr. R. D. Gaul, Director, LRAPP	1
Bay St. Louis, Mississippi, 39529	
Director Naval Research Laboratory ATTN: Technical Information Division	1
Code 5300	1
Code 5320, Mr. J. M. Headrick	1
Code 5400/5432C	1
Code 5464, Dr. J. R. Davis	1
Washington, D.C. 20390	
Commander Naval Security Group Headquarters ATTN: C3I Advisory Board, NRAC	1
3801 Nebraska Avenue, N.W. Washington, D.C. 20390	
Commander Naval Weapons Center ATTN: Code 3524, Mr. R. S. Hughes	1
Code 127, Mr. D. Witcher	1
China Lake, California 93555	
Officer-in-Charge Navy Field Operational Intelligence Office Fort Geo. G. Meade, Maryland 20755	1
Director Navy Ocean Surveillance Information Center Suitland, Maryland 20390	1
Commandant of the Marine Corps ATTN: Code RD-1, Dr. A. L. Slafkosky	1
Washington, D.C. 20380	
Center for Naval Analyses ATTN: Dr. Gary Phillips	1
1401 Wilson Boulevard Arlington, Virginia 22209	

Organization	Number of Copies
DEPARTMENT OF THE AIR FORCE	
Office of the Assistant Secretary of the Air Force (R&D) ATTN: SAF/RD, Dr. Albert C. Vosburg	1
Pentagon, Room 4D977 Washington, D.C. 20330	
Headquarters, USAF ATTN: AF RDPE, Lt. Col. J. Wheeler	1
AFINY	1
Pentagon Washington, D.C. 20330	
Headquarters Research and Technology Division Air Force Systems Command ATTN: DLC	1
SDED	1
Andrews AFB, Washington, D.C. 20331	
Headquarters Electronic Systems Division Air Force Systems Command ATTN: OCS, 414L SPO	3
OCSE	1
OCSX	1
Hanscom AFB, Massachusetts 01731	
Headquarters Air Force Geophysics Laboratory (AFSC) ATTN: PHI	1
Hanscom AFB, Massachusetts 01731	
Headquarters Rome Air Development Center ATTN: OCSE	1
OCSL	1
Griffiss AFB, New York 13442	
Headquarters Rome Air Development Center ATTN: EEP	1
Hanscom AFB, Massachusetts 01731	
Headquarters Foreign Technology Division Air Force Systems Command ATTN: ENDP	1
ENDA	1
PDJL	1
Wright Patterson AFB, Ohio 45433	
Headquarters Aerospace Defense Command ATTN: XPAS	4
Ent AFB, Colorado 80912	

DISTRIBUTION LIST (Continued)

Organization	Number of Copies
Headquarters, SAC ATTN: DOKS XPF Offutt AFB Omaha, Nebraska 68113	 1 1
Headquarters 4754 RADES/DVS ATTN: Dr. George Parker Hill AFB, Utah 84401	1
Headquarters Air Weather Service ATTN: AWS/DNP Scott AFB, Illinois 62265	1
Headquarters USAF Security Service ATTN; USAFSS/XRS San Antonio, Texas 78241	1
DEPARTMENT OF THE ARMY	
Director Ballistic Missile Defense Advanced Technology Center ATTN: BMDATC-D, Mr. Frank L. Brown Huntsville, Alabama 35807	1
Commander U.S. Army INSCOM Arlington Hall Station ATTN: IARDA-OS Arlington, Virgonia 22212	1
Commander U.S. Army Garrison Vint Hill Farms Station ATTN: IAVOP-AF Warrenton, Virginia 22186	1
OTHER	
Barry Research ATTN: Dr. R. B. Fenwick 767 North Mary Sunnyvale, California 94085	1
Environmental Research Institute of Michigan P. O. Box 618 Ann Arbor, Michigan 48107	1
General Electric Company Heavy Military Electronics System ATTN: Mr. Gary R. Nelson P. O. Box 1122, Court Street Plant 4-1 Syracuse, New York 13201	1
GTE Sylvania, Inc. Electronic Systems Group - ED ATTN: Mr. J. Page 77 A Street Needham, Massachusetts 02194	1
GTE Sylvania, Inc. Electronic Systems Croup - WD ATTN: Mr. Larry Fowler P. O. Box 205 Mountain View, California 94040	1
Massachusetts Institute of Technology Lincoln Laboratory ATTN: Dr. R. M. O'Donnell, Group 43 P. O. Box 73 Lexington, Massachusetts 02173	1
MITRE Corporation ATTN: Mr. William Talley Mr. Samuel Hunt Mr. D. J. Marino Route 62 and Middlesex Turnpike Bedford, Massachusetts 01730	 1 1 1
NOAA Laboratories ATTN: ERL R45x5, Dr. Donald Barrick Boulder, Colorado 80302	1
Radio Corporation of America ATTN: Dr. R. W. Roop Borton Landing Road Moorestown, New Jersey 08057	1
RAND Corporation ATTN: Dr. Cullen Crain 1700 Main Street Santa Monica, California 90406	1
Raytheon Company Boston Post Road ATTN: Mr. L. C. Edwards Wayland, Massachusetts 01778	1
Raytheon Company Sudbury Engineering Facility ATTN: Mr. D. Odom 528 Boston Post Road Sudbury, Massachusetts 01776	1
Riverside Research Institute ATTN: Mr. R. Mastrandrea 80 West End Avenue New York, New York 10023	1

ESD 414L SPO/
ONR NR 088-076/SRI 4062/L Series
Revised January 1978

DISTRIBUTION LIST (Concluded)

Organization	Number of Copies
Sanders Associates ATTN: Mr. Sidney M. Bennett Mr. Robert A. Palmer 95 Canal Street Nashua, New Hampshire 03060	 1 1
Stanford Research Institute ATTN: Mr. John Schlobohm/Dr. John Am`s 333 Ravenswood Avenue Menlo Park, California 94025	 1
U. S. Department of Commerce Office of Telecommunications ATTN: Dr. William Utlaut Mr. L. H. Tventen, 4401.210 Institute for Telecommunication Science Boulder, Colorado 80302	 1 1
University of Colorado Office of Contracts and Grants ATTN: Ms. Virginia Stone for Prof. Lloyd J. Griffiths Administrative Annex, Willard 380 Boulder, Colorado 80302	 1

ESD 414L SPO/
ONR NR 088-076/SRI 4062/L Series
Revised January 1978